

# Hadron Diffractive Processes: the Structure of Soft Pomeron and Colour Screening

L.G.Dakhno<sup>1)</sup> and V.A.Nikonov<sup>2)</sup>

St.Petersburg Nuclear Physics Institute,  
Gatchina, St.Petersburg 188350, Russia

<sup>1)</sup> dakhno@hep486.pnpi.spb.ru

<sup>2)</sup> nikon@rec03.pnpi.spb.ru

## Abstract

On the basis of the experimental data on diffractive processes in  $\pi p$ ,  $pp$  and  $p\bar{p}$  collisions at intermediate, moderately high and high energies, we restore the scattering amplitude related to the  $t$ -channel exchange by vacuum quantum numbers by taking account of the diffractive  $s$ -channel rescatterings. At intermediate and moderately high energies, the  $t$ -channel exchange amplitude turns, with a good accuracy, into an effective pomeron which renders the results of the additive quark model. At superhigh energies the scattering amplitude provides a Froissart-type behaviour, with an asymptotic universality of cross sections such as  $\sigma_{\pi p}^{tot}/\sigma_{pp}^{tot} \rightarrow 1$  at  $s \rightarrow \infty$ . The quark structure of hadrons being taken into account at the level of constituent quarks, the cross sections of pion and proton (antiproton) in the impact parameter space of quarks,  $\sigma_{\pi}(\vec{r}_{1\perp}, \vec{r}_{2\perp}; s)$  and  $\sigma_p(\vec{r}_{1\perp}, \vec{r}_{2\perp}, \vec{r}_{3\perp}; s)$ , are found as functions of  $s$ . These cross sections implicate the phenomenon of colour screening: they tend to zero at  $|\vec{r}_{i\perp} - \vec{r}_{k\perp}| \rightarrow 0$ . The effective colour screening radius for pion (proton) is found for different  $s$ . The predictions for the diffractive cross sections at superhigh energies are presented.

PACS: 14.20.Dh, 14.40.Aq, 13.85.Dz, 13.85.1g

## 1 Introduction

The investigation of diffractive processes at moderately high and high energies turned rather long ago into the study of the  $t$ -channel structure of the amplitude with vacuum quantum numbers (pomeron). The understanding of the  $t$ -channel exchange amplitude grew up parallel with the growth of energies of the colliding particles studied in the

experiment. The main characteristics of the soft pomeron are its intercept and proper size. A particular feature of the QCD pomeron is the colour screening phenomenon.

In the latest decade it became clear that an understanding of the  $t$ -channel structure of the amplitude is not enough for the description of diffractive processes at high and superhigh energies, because the  $s$ -channel diffraction rescatterings play here a crucial role. The present paper is devoted to the study of the soft pomeron (or Strong-QCD pomeron), with a simultaneous  $s$ -channel unitarization of the amplitude due to the account for diffractive rescatterings.

The paper is organized as follows. In section 2 a brief survey of the problem is presented, with an emphasis to various approaches to the Strong-QCD pomeron. In section 3, in the framework of generalized eikonal approach which includes the  $s$ -channel diffractive rescatterings in the leading order terms of the  $1/N_c$ -expansion, the description of the experimental data is carried out for the  $p\bar{p}(pp)$ ,  $\pi p$  and  $\gamma p$  soft diffractive processes. In Conclusion we summarize the results underlining our vision of diffractive processes. In Appendix A the formulae for diffractive amplitudes are derived, the basic points of the generalized eikonal approach being emphasized. Appendix B is devoted to the three-reggeon amplitude **PGG** which is responsible for the colour screening. In Appendix C the pomeron-meson amplitude is presented in terms of the light-cone variables.

## 2 Strong-QCD pomeron

**a. Pomeron intercept.** The range of intermediate and moderately high energies is well described by the  $t$ -channel pomeron with an intercept  $\alpha_P(0) = 1$  (the pomeron of Gribov - Chew - Frautschi (GCF) [1]). Still, with the energy increase it became obvious that the experimental data do not obey the GCF pomeron: Kaidalov and Ter-Martirosyan (KT) [2] suggested a supercritical pomeron with an intercept  $\alpha_P(0) = 1 + \Delta$  where  $\Delta > 0$ , that gives  $\sigma^{tot} \sim s^\Delta$ ; in fitting to data the magnitude  $\Delta \simeq 0.12$  was found. Donnachie and Landshoff (DL) [3] succeeded in the description of a wide range of experimental data on the diffractive processes using a supercritical pomeron with  $\Delta \simeq 0.08$ . As was obvious from the very beginning, the one-pomeron exchange amplitude with  $\Delta \sim 0.1$  (KTDL pomeron) is applicable in a restricted region of energies. With the energy growth, the one-pomeron exchange amplitude with  $\Delta \sim 0.1$  violates the unitarity requirement, for the maximal allowed growth should be consistent with the Froissart limit which provides a weaker growth,  $\sigma^{tot} \sim \ln^2 s$ .

In Refs. [4, 5], it was argued that the pomeron with  $\Delta = 0.08$  is a universal object capable to describe the soft diffraction and small- $x$  deep inelastic processes at moderately high and high energies. However, the value  $\Delta \simeq 0.08$  contradicts the DESY data on vector-meson electroproduction at the invariant energies  $W = 10 - 200$  GeV [6]. For this process and small- $x$  deep inelastic scattering the value  $\Delta \sim 0.2 - 0.3$  was found (see [7] and references therein).

In the present paper we underline that the value  $\Delta \sim 0.1$  does not provide a self-consistent description of the diffractive scattering data even at moderately high energies. The large diffractive cross section (its magnitude is nearly one half of  $\sigma^{tot}$ , as was stressed long ago [8]) results in large  $s$ -channel–unitarity corrections. In the complex- $j$  plane, they generate branching points of a considerable contribution, and these branching points are not cancelled by other subprocesses. The total contribution which comes from the pole and branching points requires  $\Delta > 0.1$  [9, 10].

**b. Soft-pomeron size.** Pomeron is mainly a gluonic system, and this defines its properties. One of the most important characteristics of the pomeron, on which the physics of the diffractive processes is founded, is the pomeron size. The partons of the gluonic ladder, which forms a pomeron, saturate a disk in the impact parameter space. The radius of the disk increases infinitely with  $s$ , and it is the pomeron slope,  $\alpha'_P(0)$ , which determines the disk size at fixed  $s$ . As it follows from the experiment, the pomeron slope is not large at modern high energies,  $\alpha'_P(0) \sim 0.2 \text{ (GeV/c)}^{-2}$  [11]. It can be compared with the slope of the  $\rho$ -meson trajectory – this slope being a typical hadronic value is considerably larger:  $\alpha'_\rho(0) \simeq 1 \text{ (GeV/c)}^{-2}$ . For the pomeron represented by the gluon ladder of Fig. 1a, the slope  $\alpha'_P(0)$  is determined by the size of the gluon plaquet which is a constructive element for this ladder, see Fig. 1b. As was stressed in Ref. [12], the small size of this plaquet can be affected by a comparatively large mass of the effective gluon (the soft gluon), this mass being of the order of  $0.7 - 1.0 \text{ GeV}$ .

The prompt evaluation of the effective gluon mass is possible in radiative  $J/\psi$  and  $\Upsilon$  decays. The estimation of the effective gluon mass firstly performed by Parisi and Petronzio [13] for the decay  $J/\psi \rightarrow \gamma + gg$  provided the value  $m_g \simeq 800 \text{ MeV}$ . The analysis [14] of more copious data gave  $m_g \simeq 800 \text{ MeV}$  for the reaction  $J/\psi \rightarrow \gamma + gg$  and  $m_g = 1100 \text{ MeV}$  for  $\Upsilon \rightarrow \gamma + gg$ .

The glueball physics enlightens the problems of soft gluodynamics as well. Within the lattice calculus, the following values were obtained for the mass of the lightest scalar glueball:  $m_{\text{scalar glueball}} = 1549 \pm 53 \text{ MeV}$  [15] and  $1740 \pm 71$  [16]. Experimental data also indicate the existence of the scalar-isoscalar state in the mass region  $1300 - 1600 \text{ MeV}$ : this state being an excess for the quark-antiquark nonet systematics is a good candidate for the lightest scalar glueball [17, 18]. These results support a comparatively large value of the effective gluon mass:  $m_g \sim m_{\text{scalar glueball}}/2 \sim 650 - 800 \text{ MeV}$ . Moreover, in line with this discussion, lattice calculations [16] resulted in a small size of the lightest scalar gluodynamic glueball,  $\langle r^2 \rangle_{\text{glueball}} \simeq 0.1 \text{ fm}^2$ .

In the bootstrap-type model [19], when the forces responsible for the meson formation are determined by the exchange of both effective gluon and mesons, the  $q\bar{q}$ -spectroscopic calculations of mesons from the low-lying multiplets  $1^1S_0 q\bar{q}$ ,  $1^3S_1 q\bar{q}$  and  $1^3P_1 q\bar{q}$  required the massive effective gluon,  $m_g \simeq 700 \text{ MeV}$ , in an agreement with the above-discussed values.

The estimation of the gluon mass within perturbative QCD [20] yielded the value of the same order:  $m_g = 1.5^{+1.2}_{-0.6} \text{ GeV}$ , and recent lattice calculation [21] provided us with  $m_g \simeq 0.8 \text{ GeV}$ .

The quark model had a striking success in the description of hadron collisions at

intermediate and moderately high energies. The pomeron size is crucial characteristics for the quark model, for only with a small-size pomeron the additivity of the scattering amplitudes occurs. This was formulated rather long ago [22]. At 70's and the beginning of 80's, parallel with accumulating experimental data, the arguments in favour of pomeron's small size grew up [23]; they were summarized in [24]. Later on, the small-size pomeron was named a point-like pomeron [25].

An opposite point of view concerning the pomeron had been developed in the approach initiated by Low and Nussinov [26], where the  $t$ -channel exchange with vacuum quantum numbers was treated as an exchange of the two massless gluons (see Figs. 1c,d, where typical diagrams for meson–meson scattering are drawn). The  $t$ -channel massless gluons emulated a large radius for the  $t$ -channel interaction, thus forming a large-size pomeron. A noticeable advantage of this approach consisted in a formulation of the colour screening phenomenon for colliding quarks: the diagrams of Figs. 1c,d cancelled each other at  $|\vec{r}_{1\perp} - \vec{r}_{2\perp}| \rightarrow 0$  ( $\vec{r}_{1\perp}$  and  $\vec{r}_{2\perp}$  are impact parameters of quark and antiquark of a meson represented by the upper block). Later on, the colour screening phenomenon became a subject of a special discussion and gave rise to the search for the colour transparency, see [27] and references therein. In the Low–Nussinov model the large radius of the two-gluon interaction led to the dipole structure of the scattering amplitude. As a result,  $\sigma_{\pi p}^{tot}$  was proportional to the pion mean radius squared,  $\langle r_\pi^2 \rangle$ , and  $\sigma_{pp}^{tot}$  was proportional to  $\langle r_p^2 \rangle$ , hence  $\sigma_{\pi p}^{tot}/\sigma_{pp}^{tot} \simeq \langle r_\pi^2 \rangle / \langle r_p^2 \rangle \simeq 2/3$ , in qualitative agreement with the experimental data [28].

However, one should stress that a direct use of the massless-gluon exchange violated analytic properties of the scattering amplitude: the amplitude singularity appeared at  $t = 0$  that made the discontinuity unequal to zero at  $t > 0$ , namely,  $disc_t A_{\pi p, two-gluon\ exchange}^{el} \neq 0$  at  $0 < t < 4\mu_\pi^2$ , while actually  $disc_t A_{\pi p}^{el}$  appears only at  $t > 4\mu_\pi^2$ . The region of small positive  $t$  is in the closest vicinity to the physical region of diffractive processes, so the violation of analyticity looks menacing here. In [29], in order to restore the analyticity for the two-gluon exchange diagram, a cutting was suggested, with  $t_{cut} \sim 4\mu_\pi^2$ ; still, this parameter, as the effective gluon mass estimation tells us, must be greater:  $t_{cut} \sim 2 \text{ GeV}^2$ .

**c. Colour screening phenomenon.** The problem of taking account of the colour screening for quasi–point-like pomeron was discussed in [12], where Lipatov's perturbative pomeron [30] has been used as a guide. The figure 1e to f demonstrates different couplings of the Lipatov-type pomeron to meson quarks: just these two types of a coupling provide the colour screening of meson quarks for the soft pomeron. In further works [31, 32], the problem of whether the colour screening was inherent to Lipatov's pomeron has been discussed in details.

According to [9, 10], the corresponding meson–pomeron and proton–pomeron amplitudes have the following structure:

$$\begin{aligned} & \rho(\vec{b} - \vec{r}_1) + \rho(\vec{b} - \vec{r}_2) - 2\rho(\vec{b} - \frac{\vec{r}_1 + \vec{r}_2}{2}) \exp(-\frac{(\vec{r}_1 - \vec{r}_2)^2}{4r_{cs}^2}), \\ & \Sigma_{i=1,2,3} \rho(\vec{b} - \vec{r}_i) - \Sigma_{i \neq k} \rho(\vec{b} - \frac{\vec{r}_i + \vec{r}_k}{2}) \exp(-\frac{(\vec{r}_i - \vec{r}_k)^2}{4r_{cs}^2}). \end{aligned} \quad (1)$$

Here  $\rho(\vec{b})$  is the pomeron amplitude in the impact parameter space,  $\rho(\vec{b}-\vec{r}_{1\perp})$  corresponds to the pomeron-quark vertex as is shown in Fig. 1e, where the pomeron interacts with one quark only, the term  $\rho(\vec{b}-\vec{r}_{2\perp})$  relates to the second quark; the last term corresponds to the diagram of Fig. 1f where the pomeron interacts with two quarks (see Appendices A, B, C for details). In the Lipatov-type pomeron, the  $t$ -channel gluons are reggeized [33], and the intercept of reggeized gluon is close to the unity, namely,  $\alpha_{gluon}(0) = 1 - \Delta_{gluon}$ , where  $\Delta_{gluon}$  is small. The proximity  $\alpha_{gluon}(0) \simeq 1$  is an essential point for equation (1); we shall discuss it in Appendix B.

Actually, the equation (1) does not specify the pomeron size. A large pomeron size responds to the case when one can neglect the  $r_{i\perp}$ -dependence in the pomeron amplitude,  $\rho(\vec{b}-\vec{r}_i) \simeq \rho(\vec{b})$ , while the exponent is expanded in a series with respect to a small magnitude  $(\vec{r}_{1\perp}-\vec{r}_{2\perp})^2/4r_{cs}^2$  (the value  $(\vec{r}_{1\perp}-\vec{r}_{2\perp})^2$  is restricted by meson size, and the colour screening parameter,  $r_{cs}^2$ , is assumed to be large). The first non-vanishing term of a series is proportional to  $2(\vec{r}_{1\perp}-\vec{r}_{2\perp})^2$  for meson and  $(\vec{r}_{1\perp}-\vec{r}_{2\perp})^2 + (\vec{r}_{2\perp}-\vec{r}_{3\perp})^2 + (\vec{r}_{1\perp}-\vec{r}_{3\perp})^2$  for proton that, after averaging over the meson (proton) wave functions squared, results in the factor  $\langle r^2 \rangle_{meson}$  and  $\langle r^2 \rangle_{proton}$ , in a complete similarity to the two-gluon exchange model. But from now on the similarity ends, for the amplitude (1) has as a factor the pomeron amplitude  $\rho(b)$ , while for the two-gluon exchange model one has gluon propagators.

For a small-size pomeron, the ratio  $r_{cs}^2 / \langle r^2 \rangle_{meson}$  is small, so the last term in (1), which implies the colour screening, is small everywhere but for a region where meson quarks are in a squeezed configuration:  $|\vec{r}_{1\perp}-\vec{r}_{2\perp}| \leq r_{cs}$ . At the same time, the contribution of two first terms, which correspond to the impulse approximation diagrams, is significant everywhere where meson wave function dominates. In such a way, the small-size pomeron justifies additive quark model at moderately high energies; in particular, it leads to the ratio  $\sigma^{tot}(\pi p)/\sigma^{tot}(pp) \simeq 2/3$  in accordance with the pion/proton constituent quark numbers. Moreover, the colour screening term in (1), though comparatively small, allows one to explain the deviation from additivity within the constituent quark model at moderately high energies, that was a puzzle rather long ago. Namely, the ratio  $\sigma^{tot}(\pi p)/\sigma^{tot}(pp)$  is slightly less than  $2/3$  (experimentally it is  $\frac{2}{3}(1-\delta)$ , with  $\delta \simeq 0.1$ ). The Glauber rescatterings calculated within constituent quark model (see Ref. [34]) do not help providing  $\delta \simeq -0.1$ . This is understandable, for the Glauber screening is more significant for systems with larger number of constituents, that is for the proton. Therefore, the deviation of the cross section ratio from  $2/3$ , though small, is of a principal importance. It was suggested in [23] that just three-reggeon diagrams with pomeron and two colour reggeons are responsible for  $\delta > 0$ . The calculations of diffractive processes performed in [12] fortify this idea specifying colour reggeons to be reggeized gluons.

Using the language of reggeon exchanges, the impulse approximation diagrams of the type of Fig. 1e can be represented as diagrams of Figs. 2a,b, so the diagram of Fig. 1f which provides the colour screening is re-drawn as Fig. 2c; the shaded block of Fig. 2d represents the whole pomeron-meson vertex. Here **P** stands for the pomeron and **G** for reggeized gluon. In such a way the diagram responsible for the colour screening (Fig. 2c) is the three-reggeon diagram **PGG**. Likewise, the pomeron-nucleon amplitude is shown

in Fig. 2e to i, with all possible couplings of reggeized gluons  $\mathbf{G}$  to nucleon quarks, thus granting the colour screening.

**d. The  $s$ -channel unitarity and soft primary pomeron.** Within the one-pomeron exchange approach shown in Fig. 2 the calculations of the  $pp$  and  $\pi p$  scattering amplitudes have been performed in [12] for  $\sigma^{tot}$  and  $d\sigma^{el}/dt$  in the energy range  $p_{lab} \simeq 200 - 300$  GeV: this is just the region where  $\sigma_{\pi p}^{tot}$  and  $\sigma_{pp}^{tot}$  are almost energy-independent, that corresponds to  $\alpha_P(0) \simeq 1$ . Naively, the problem of extending the model to the region of higher energies looked rather simple: one should introduce  $\Delta$  of the order of 0.1, following the suggestion of Refs. [2, 3], and evaluate the corrections related to the two-pomeron exchange (these corrections are to be taken into account, because elastic and diffractive cross sections,  $\sigma^{el}$  and  $\sigma^{DD}$ , are determined by the imaginary parts of the two-pomeron exchange diagrams, and they are not small). However, the realization of this program with  $\Delta \simeq 0.08$  faced a phenomenon which may be called a hidden unitarity violation: the description of experimental data with both one-pomeron (Fig. 3a) and two-pomeron exchanges (diagrams of Fig. 3b type) requires  $\Delta$  significantly larger than 0.08. The introduction of triple rescatterings (Fig. 3c), etc. results in the subsequent increase of  $\Delta$ ; so one may conclude that the amplitude with  $\Delta = 0.08$  is not self-consistently unitary to agree with the experiment even at moderately high energies. The unitary amplitude which takes into account a full set of the  $s$ -channel rescattering diagrams (Fig. 3) and describes the available high-energy experimental data requires [10]:

$$\Delta = 0.29. \quad (2)$$

We refer to the soft pomeron with  $\Delta \simeq 0.3$  as a primary one. A significant increase of  $\Delta$  as a result of the  $s$ -channel rescatterings is due to the large contribution of diffractive processes: even at moderately high energies the diffractive processes provide nearly a half of total cross section [8], and their rate approaches 1/2 with the energy growth. A large rate of diffractive processes undermines the idea thoroughly accepted at the early stage of the pomeron study that the  $s$ -channel unitarity of the scattering amplitude is mainly due to the truly inelastic processes related to a pomeron cutting.

Fitting to experimental data on total and elastic cross sections at high energies [10] provides us with the characteristics of the primary pomeron strikingly close to the characteristics of Lipatov's one [30]. Recall that the behaviour of amplitudes related to the diffractive hadronic processes is governed by singularities in the complex plane of the angular momentum  $j$ . The pQCD pomeron in the leading-logarithm approximation is a set of ladder diagrams with the reggeized  $t$ -channel gluons, see Fig. 1a (the ladder diagram representation of the pQCD-pomeron occurs with a special choice of the spin structure of the three-gluon vertex, the gluons being reggeized). Within pure pQCD calculus, the corresponding leading singularity in the  $j$ -plane is the branching point at  $j = 1 + \Delta_{BFKL}$ , where  $\Delta_{BFKL} = (g/\pi)^2 3 \ln 2 \simeq 0.5$  (BFKL-pomeron [33, 35]). It is necessary to mention the latest next-to-leading order ( $\alpha_s^2$ ) calculations of  $\Delta_{BFKL}$  [36] which provided the value  $\Delta_{BFKL} \simeq 0.1 - 0.2$ , though it might be probable that the next correction, of the order of  $\alpha_s^3$ , would result in a value  $\Delta_{BFKL} \simeq 0.3 - 0.4$  [37].

The application of QCD-pomeron to phenomenological calculations makes it urgent to

consider the gluon virtual momenta close to those used in the leading-logarithm approximation. In [30] the virtualities of such a type have been effectively taken into account with the help of a boundary condition, together with the constraint ensured by the asymptotic freedom of QCD. The pomeron obtained in such a way, Lipatov's pomeron, is an infinite set of poles in the region  $1 < j \leq 1 + \Delta$ , and there exists a constraint for the leading pole intercept:  $\Delta \geq 0.3$ .

Coming back to the results of [10], the vacuum singularity of the primary pomeron has been approximated in the  $j$ -plane by the two poles:

$$j = 1 \quad \text{and} \quad j = 1 + \Delta \quad \text{with} \quad \Delta = 0.29, \quad (3)$$

following the idea [29] of the two-pole approximation of Lipatov's pomeron.

The value  $\Delta \simeq 0.3$  obtained from the fit of total and elastic  $\pi p$  and  $pp$  processes is on the lower boundary of the intercept of Lipatov's pomeron. Moreover, the small value of the primary-pomeron slope,  $\alpha'_P(0)$ , supports the idea about its small size. It was found [10] for the primary pomeron:

$$\alpha'_P = 0.112 \text{ (GeV/c)}^{-2}. \quad (4)$$

Another characteristics of the primary pomeron, that is the colour screening radius  $r_{cs}$ , also manifests the small size of the primary pomeron [10]:

$$r_{cs} = 0.17 \text{ fm}. \quad (5)$$

One may suggest that just the small size of the primary pomeron makes its properties close to the characteristics to the Lipatov's pomeron.

In the present paper we have extended the applicability region, having included the intermediate energy region  $p_{lab} \simeq 50 - 200 \text{ GeV/c}$  into consideration. This requires an additional pole:

$$j = 1 - \Delta', \quad \text{with} \quad \Delta' > 0. \quad (6)$$

However, this did not affect the characteristics of the two leading poles (3).

**e. Superhigh energies and the Froissart limit.** At superhigh energies, the diffractive cross section approaches its asymptotics determined by a full set of multipomeron exchanges, which examples are shown in Fig. 3. In the impact parameter space, the interaction region is a black disk, with the radius growing as  $\ln s$  (Froissart limit). At  $\sqrt{s} \geq 500 \text{ GeV}$ , in the leading-logarithm approximation (that means  $R_{disk} \sim r_{disk} \ln s$ ), the  $p\bar{p}$  and  $\pi p$  cross sections behave as follows [10]:

$$\begin{aligned} \sigma_{\pi p}^{tot} &\simeq \sigma_{p\bar{p}}^{tot} \simeq 2\pi r_{disk}^2 \ln^2 s, \\ \sigma_{\pi p}^{el} &\simeq \sigma_{p\bar{p}}^{el} \simeq \pi r_{disk}^2 \ln^2 s, \\ \frac{d\sigma_{\pi p}^{el}}{dq_{\perp}^2} &\simeq \frac{d\sigma_{p\bar{p}}^{el}}{dq_{\perp}^2} \simeq \frac{\pi}{4} r_{disk}^4 \ln^4 s \exp\left(-\frac{1}{4} r_{disk}^2 \ln^2 s \cdot q_{\perp}^2\right), \end{aligned} \quad (7)$$

where  $r_{disk}^2 \simeq 0.051 \text{ mb} = (0.071 \text{ fm})^2$ . Generally, the scattering off the black disk leads to the Bessel-type amplitude oscillations in  $q_\perp^2$ ; still, as we consider here the amplitude in the region of small  $q_\perp^2$ , the exponential representation is valid. It should be emphasized that the late start of the asymptopia is caused by small  $r_{disk}^2$ : this magnitude almost coincides with  $\alpha'_P = 0.112 \text{ (GeV/c)}^{-2} = (0.066 \text{ fm})^2$ , see (4). The dimensional characteristics of the primary pomeron ( $\alpha'_P$ ,  $r_{cs}^2$ ,  $r_{disk}^2$ ) obtained by fitting to data are rather small and of the same order: we consider this as a manifestation of a comparatively large mass of the effective gluon. The idea that the gluonic structure of the high-energy  $t$ -channel exchanges results in a late asymptopia was discussed in Ref. [38].

At lower energies,  $\sqrt{s} \leq 500 \text{ GeV}$ , the terms proportional to  $\ln s$  become important in diffractive cross sections, and at  $\sqrt{s} < 15 \text{ GeV}$  the term  $\sim 1/s^{\Delta'}$  is seen.

**f. Intermediate and moderately high energies.** The analysis of diffractive processes at intermediate and moderately high energies,  $p_{lab} \sim 50 - 100 \text{ GeV/c}$ , is of a great interest:

- (i) The pomeron exchanges dominate at these energies, so expanding our approach to this energy region makes it possible to resolve more precisely the  $j$ -plane pomeron singularities.
- (ii) This energy region was discussed in the literature as a suitable one for the study of colour transparency. For quantitative estimation of colour transparency, the colour screening radius for the pomeron interaction should be known as a function of energy: the analysis of diffractive processes can give such information.
- (iii) The additive quark model provides rather good description of data at intermediate and moderately high energies. So, it is very instructive to trace the transitions of diffractive amplitudes from superhigh energies, where hadron amplitudes are universal, to the region, where the quark additivity works.

It should be stressed once again that coming from superhigh energies, where pomeron parameters are properly determined, to the region of moderate energies, where non-leading trajectories are significant, allows us to evaluate more precisely the contributions of the non-leading terms. This evaluation makes it possible to fix the beginning of a pure pomeron contribution.

**g. Eikonal and generalized eikonal approaches.** The eikonal approach allows one to resolve the problem of the  $s$ -channel unitarization of the diffractive amplitudes for  $\Delta > 0$ . The eikonal approach was applied to the  $\pi p$  and  $pp$  scattering amplitudes at high energies in [39, 40]. However, the classic eikonal formulae do not take into consideration the diffractive production processes in the intermediate states, although this contribution is of the same order as the classic eikonal rescatterings. In [9, 10] a generalized eikonal approach was developed in which the diffractive processes have been considered at the constituent quark level: this allows us to take account of all diffractive processes which are directly related to the disintegration of colliding hadrons. This is due to the quark-hadron duality: the  $q\bar{q}$ -state (see Fig. 4a) is equivalent to a full set of hadron states (Fig. 4b,c).

The  $1/N_c$  expansion rules [41] allow us to believe that generalized eikonal is a reasonable approximation for the description of diffractive processes caused by primary pomeron.



The fact is that the coupling of the primary pomeron to hadron is suppressed as  $1/N_c$ , but this suppression is compensated by the increase of  $s^\Delta$ . Multi-pomeron vertices, like **PPP** or **PPPP** of Fig. 4d,e, are not included into generalized eikonal approach because their contribution is even more suppressed: the vertex  $g_{\mathbf{PPP}}$  is of the order of  $1/N_c$  and  $g_{\mathbf{PPPP}} \sim 1/N_c^2$ .

### 3 Diffractive processes: the comparison with experiments

In this section, in the framework of generalized eikonal approach, we describe the elastic scattering amplitude for the  $pp(\bar{p}p)$ ,  $\pi p$  and  $\gamma p$  reactions. We consider  $Im A^{el}(q^2 = 0) \sim \sigma^{tot}$ ,  $\sigma^{el}$ ,  $\rho = Re A^{el}/Im A^{el}$  and the elastic scattering slope  $B$  over wide energy range, starting from  $p_{lab}(pp) = 50$  GeV/c, and restore the characteristics of the primary pomeron.

The diffraction dissociation cross section related to the dissiciation of the colliding hadrons has been calculated and compared with the experimental data for  $pp \rightarrow pX$ , that allows us to estimate the cross section which is due to the three-pomeron vertex **PPP**.

**a. Total and elastic cross sections.** We refer to Appendices A and B for the derivation of formulae written below. Our approach is applied to  $\sigma_{p\bar{p}(pp),\pi p}^{tot,el}$ , the main goal is to extract the parameters of the soft primary pomeron from the comparison with experimental data. The following formulae describe total and elastic cross sections of the colliding hadrons  $A$  and  $B$ :

$$\sigma_{AB}^{tot} = 2 \int d^2b \int dr' \varphi_A^2(r') dr'' \varphi_B^2(r'') \left[ 1 - \exp\left(-\frac{1}{2}\chi_{AB}(r', r'', b)\right) \right], \quad (8)$$

$$\sigma_{AB}^{el} = \int d^2b \left\{ \int dr' \varphi_A^2(r') dr'' \varphi_B^2(r'') \left[ 1 - \exp\left(-\frac{1}{2}\chi_{AB}(r', r'', b)\right) \right] \right\}^2. \quad (9)$$

The expression  $dr \varphi_{A,B}^2(r)$  stands for quark densities of the colliding hadrons  $A$  and  $B$  which depend on the transverse coordinates. The pion and proton densities are defined as follows:

$$\begin{aligned} dr \varphi_\pi^2(r) &\equiv d^2r_1 d^2r_2 \delta^2(\vec{r}_1 + \vec{r}_2) \varphi_\pi^2(r_1, r_2), \\ dr \varphi_p^2(r) &\equiv d^2r_1 d^2r_2 d^2r_3 \delta^2(\vec{r}_1 + \vec{r}_2 + \vec{r}_3) \varphi_p^2(r_1, r_2, r_3), \end{aligned} \quad (10)$$

where  $r_i$  is transverse coordinate of the quark; the averaging over longitudinal variables is performed. The proton and pion quark densities are determined by their form factors; this is discussed in Appendix A.

The profile-function  $\chi_{AB}$  describes the interaction of quarks of colliding hadrons via the pomeron exchange as follows:

$$\chi_{AB}(r', r'', b) = \int db' db'' \delta^2(b - b' + b'') \rho_A(b', r') \rho_B(b'', r''). \quad (11)$$

The functions  $\rho_{A,B}$  stand for the amplitudes of the one-pomeron exchange:

$$\rho_\pi(\vec{r}, \vec{b}) = \rho(\vec{b} - \vec{r}_1) + \rho(\vec{b} - \vec{r}_2) - 2\rho\left(\vec{b} - \frac{\vec{r}_1 + \vec{r}_2}{2}\right) \exp\left(-\frac{(\vec{r}_1 - \vec{r}_2)^2}{4r_{cs}^2}\right),$$

$$\rho_p(\vec{r}, \vec{b}) = \sum_{i=1,2,3} \rho(\vec{b} - \vec{r}_i) - \sum_{i \neq k} \rho(\vec{b} - \frac{\vec{r}_i + \vec{r}_k}{2}) \exp(-\frac{(\vec{r}_i - \vec{r}_k)^2}{4r_{cs}^2}). \quad (12)$$

Functions  $\rho_\pi$  and  $\rho_p$  tend to zero at  $|\vec{r}_{ij}| \rightarrow 0$ . We perform calculations in the centre-of-mass system of colliding hadrons, supposing that hadron momentum is equally shared between quarks. Then

$$\rho(b) = \frac{\sqrt{f_P(s_{qq})}}{4\pi(G + \frac{1}{2}\alpha'_P \ln s_{qq})} \exp \left[ -\frac{b^2}{4(G + \frac{1}{2}\alpha'_P \ln s_{qq})} \right], \quad (13)$$

where the pomeron-quark vertex  $\sqrt{f_P(s_{qq})}$  depends on the energy squared of the colliding quarks,  $s_{qq}$  (see Appendix A for details).

Equations (8)–(9) depend on the transverse coordinates of quarks only, though the original expressions (C.9) and (C.17) of Appendix C depend on the momentum fractions  $x_i$  of quarks of the colliding hadrons; hence  $s_{qq} = sx_i^{(\pi)}x_j^{(p)}$  for  $\pi p$  and  $s_{qq} = sx_i^{(p)}x_j^{(p)}$  for  $pp$  collisions. We put  $x_i = 1/2$  for meson and  $x_i = 1/3$  for proton assuming that hadron wave functions  $\varphi_\pi(\vec{r}, x)$  and  $\varphi_p(\vec{r}, x)$  select the mean values of  $x_i$  in the interaction blocks. A wide range of wave functions obey this assumption, for example, the wave functions of the quark spectroscopy. But the situation with the colour screening diagram **PGG** is more complicated. One should integrate over a part of the energy carried by reggeized gluons and pomeron: this spreads  $x_i$ 's of interacting quarks. However, if the intercept of the reggeized gluon  $\alpha_G(0) \simeq 1$  that is actually a requirement of the BFKL pomeron,  $x_i$  can be considered as frozen. This assumption is valid for  $0.8 < \alpha_G(0) < 1$ , that was checked by numerical calculations for realistic pion and proton wave functions. In due course, we put  $s_{qq} = s/6$  for  $\pi p$  and  $s_{qq} = s/9$  for  $pp$  collisions.

The equations (8)–(9) can be used at small momentum transfers, when real parts of the amplitude is small. We neglect the signature factor of the primary pomeron, though it can be easily restored.

The strategy for the total and elastic cross section calculations has been chosen as follows. Initially we have included into our calculation the region of high and superhigh energies. The reason is that at such energies the exchange of vacuum quantum numbers (pomeron) is the only possible, the other contributions must vanish. Under such an assumption, it is possible to restrict ourselves by the two leading trajectory only. Therefore

$$\rho_\pi(\vec{r}, \vec{b}) = \rho_\pi^{(1)}(\vec{r}, \vec{b}) + \rho_\pi^{(0)}(\vec{r}, \vec{b}), \quad (14)$$

$$\rho_p(\vec{r}, \vec{b}) = \rho_p^{(1)}(\vec{r}, \vec{b}) + \rho_p^{(0)}(\vec{r}, \vec{b}).$$

Every term  $\rho^{(0,1)}(\vec{r}, \vec{b})$  is given by (12), with its own set of parameters  $G$ ,  $\alpha'_P$ ,  $r_{cs}^2$  and  $f_P(s_{qq})$ , but for high and superhigh energies the identical sets of parameters for  $\rho^{(0)}$  and  $\rho^{(1)}$  occurred to be a good approximation:  $G^{(1)} = G^{(0)}$ ,  $r_{cs}^{(1)} = r_{cs}^{(0)}$ ,  $\alpha'_P{}^{(1)} = \alpha'_P{}^{(0)}$ , and they differ by their intercepts only.

In such a way the characteristics of the primary pomeron have been found: the supercritical parameter  $\Delta$ , parameters  $G$  and  $\alpha'_P$  for the pomeron slope, and colour screening

radius:

$$\Delta = 0.29, \quad G = 0.167 \text{ (GeV/c)}^{-2}, \quad \alpha'_P = 0.112 \text{ (GeV/c)}^{-2}, \quad r_{cs} = 0.17 \text{ fm}, \quad (15)$$

and

$$f_P(s_{qq}, q_\perp^2 = 0) = g_1^2 + g_0^2 s_{qq}^\Delta, \quad \Delta = 0.29, \quad g_0^2 = 8.079 \text{ mb}, \quad g_1^2 = 0.338 \frac{\text{mb}}{\text{GeV}^{2\Delta}}. \quad (16)$$

For the description of intermediate energies it is necessary to introduce at least one more pole  $\rho^{(-1)}(\vec{r}, \vec{b})$ , thus the whole expression becomes:

$$\begin{aligned} \rho_\pi(\vec{r}, \vec{b}) &= \rho_\pi^{(1)}(\vec{r}, \vec{b}) + \rho_\pi^{(0)}(\vec{r}, \vec{b}) + \rho_\pi^{(-1)}(\vec{r}, \vec{b}), \\ \rho_p(\vec{r}, \vec{b}) &= \rho_p^{(1)}(\vec{r}, \vec{b}) + \rho_p^{(0)}(\vec{r}, \vec{b}) + \rho_p^{(-1)}(\vec{r}, \vec{b}). \end{aligned} \quad (17)$$

In order to minimize the ambiguities, at  $p_{lab} \sim 50 - 100 \text{ GeV/c}$  the three terms in the r.h.s. of (17) are parameterized in the form (13); the parameters  $f_P(s_{qq}, q_\perp^2 = 0)$ ,  $\alpha'_P$ ,  $G$  and  $r_{cs}$  are considered as independent at different energies. As it occurred, the parameter  $\alpha'_P$  remains the same as before:  $\alpha'_P = 0.112 \text{ (GeV/c)}^{-2}$ . The values  $f_P(s_{qq}, q_\perp^2 = 0)$ ,  $G$  and  $r_{cs}$  are now energy-dependent. The function  $f_P(s_{qq}, q_\perp^2 = 0)$  is now as follows:

$$f_P(s_{qq}, q_\perp^2 = 0) = g_1^2 s_{qq}^\Delta + g_0^2 + \frac{g_{(-1)}^2}{s_{qq}^{\Delta'}}, \quad \Delta' = 1.154, \quad g_{(-1)}^2 = -44.9 \text{ mb} \cdot \text{GeV}^{-2\Delta'}. \quad (18)$$

The description of total and elastic  $p\bar{p}(pp)$  and  $\pi p$  cross sections at intermediate energies  $\sqrt{s} = 5 \div 20 \text{ GeV}$  is shown in Fig. 6a,b, together with the energy dependent parameters (Fig. 6c,d,e). The accuracy for the parameter  $G$  is not high enough (Fig. 6e): its magnitude, like  $\alpha'_P$ , can be regarded as energy-independent. It should be pointed out that the colour screening radius becomes smaller with the energy decrease; this fact supports additive quark model at moderate energies (Fig. 6d). A later (in the  $s$ -scale) onset of three-reggeon diagram **GGP** compared with the onset of one-pomeron diagram **P** results in a much smaller colour screening effects at  $\sqrt{s} \sim 5 \text{ GeV}$  (in **GGP** the energy  $\sqrt{s}$  is shared between **G** and **P**:  $\sqrt{s}m^2 = \sqrt{s_{\mathbf{G}}s_{\mathbf{P}}}$  where  $m \sim 1 \text{ GeV}$ ). In other words, the colour screening is somehow analogous to the inelastic shadowing which starts at the energies large enough to exceed the inelasticity threshold in the intermediate state. Then, with a further increase of energies, the contribution of inelastic shadowing grows, until the integration over intermediate mass is saturated by the three-pomeron peak, or — as it happens with colour screening — by **PGG** peak, which behaves like **PPP** due to the proximity of the reggeized gluon intercept to the unity. Because of this similarity, it looks natural that colour screening radius  $r_{cs}$  tends to zero with the energy decrease.

At asymptotic energies ( $\sqrt{s} \geq 500 \text{ GeV}$ ) the cross sections  $\sigma_{pp}^{tot}$  and  $\sigma_{\pi p}^{tot}$  calculated with the parameters (15) increase as  $0.32 \ln^2 s \text{ mb}$ , while the growth with energy of the elastic cross sections,  $\sigma_{pp}^{el}$  and  $\sigma_{\pi p}^{el}$ , is proportional to  $0.16 \ln^2 s \text{ mb}$ . At  $\sqrt{s} \geq 50 \text{ GeV}$ , within the 5% accuracy, the calculated total and elastic cross sections can be approximated by the following formulae:

$$\sigma_{pp}^{tot} = 49.80 + 8.16 \ln(s_{qq}/s_0) + 0.32 \ln^2(s_{qq}/s_0),$$

$$\begin{aligned}
\sigma_{\pi p}^{tot} &= 30.31 + 5.70 \ln(s_{qq}/s_0) + 0.32 \ln^2(s_{qq}/s_0). \\
\sigma_{pp}^{el} &= 8.19 + 3.027 \ln(s_{qq}/s_0) + 0.16 \ln^2(s_{qq}/s_0), \\
\sigma_{\pi p}^{el} &= 3.87 + 1.567 \ln(s_{qq}/s_0) + 0.16 \ln^2(s_{qq}/s_0).
\end{aligned} \tag{19}$$

In (19) the numerical coefficients are given in mb and  $s_0 = 10000 \text{ GeV}^2$ . Recall that  $s_{qq} = s/9$  for  $pp(p\bar{p})$  and  $s_{qq} = s/6$  for  $\pi p$  collisions.

Our predictions for LHC energies ( $\sqrt{s} = 16 \text{ TeV}$ ) are:

$$\sigma_{pp}^{tot} = 131 \text{ mb}, \quad \sigma_{pp}^{el} = 41 \text{ mb}.$$

At far asymptotic energies the ratio of total cross sections  $\sigma_{pp}^{tot}/\sigma_{\pi p}^{tot}$  tends to the unity. At these energies  $\sigma_{AB}^{el}/\sigma_{AB}^{tot} \rightarrow 1/2$  (black disk limit).

**b. Diffraction dissociation of colliding hadrons.** The following formulae stand for the diffraction dissociation processes:

$$\sigma_{AB}^{single, DD(B)} + \sigma_{AB}^{el} = \int d^2b \int dr' \varphi_A^2(r') dr'' \varphi_B^2(r'') d\tilde{r}' \varphi_A^2(\tilde{r}') \tag{20}$$

$$\begin{aligned}
&\times \left[ 1 - \exp\left(-\frac{1}{2}\chi_{AB}(r', r'', b)\right) \right] \left[ 1 - \exp\left(-\frac{1}{2}\chi_{AB}(\tilde{r}', r'', b)\right) \right], \\
\sigma_{AB}^{total \text{ diffraction}} &= \sigma_{AB}^{el} + \sigma_{AB}^{single, DD(B)} + \sigma_{AB}^{single, DD(A)} + \sigma_{AB}^{double} \\
&= \int d^2b \int dr' \varphi_A^2(r') dr'' \varphi_B^2(r'') \left[ 1 - \exp\left(-\frac{1}{2}\chi_{AB}(r', r'', b)\right) \right]^2,
\end{aligned} \tag{21}$$

where  $\sigma_{AB}^{single, DD(B)}$  describes the diffractive dissociation of a hadron B and  $\sigma_{AB}^{total \text{ diffraction}}$ , stands for total hadron diffraction.

Let it be emphasized that there are two mechanisms contributing to the diffractive dissociation cross section  $\sigma_{AB}^{single, DD(B)}$  measured at the experiment:

- (i) dissociation of a colliding hadron, see Fig. 7a, and
- (ii) partly dissociated pomeron, Fig. 7b (the cross section for the process of Fig. 7b is shown separately in Fig. 7c: it is related to the three-pomeron cut).

In the used approach the formulae (20)–(21) describe the hadron dissociation only but not the pomeron one. The calculated cross section  $\sigma_{pp}^{single, DD(p)}$  which is due to the proton dissociation is presented in Fig. 7d, and figure 7e shows the difference  $\sigma_{pp}^{single, DD(p)}(exp) - \sigma_{pp}^{single, DD(p)}(calculated)$ , the latter term given by Eq. (20). This difference stands just for the diffraction of a partly dissociated pomeron, that is the three-pomeron diagram of Fig. 7c. It should be pointed out that generalized eikonal approach allows one to calculate the other characteristics of the diffractive hadron dissociation, namely, the  $M^2$ - and  $t$ -dependences. However, such a study is beyond the scope of this article.

**c. Photon–proton total cross section and the photo-production of vector mesons.** The developed approach, which until now has been applied to the diffractive  $pp$  and  $\pi p$  cross sections, can be also applied to the reactions with a photon, that is based on the hypothesis of vector-meson dominance,  $\gamma \rightarrow V$ . Corresponding calculations have been performed for the sum of diagrams shown in Fig. 8a,b. It is assumed that the wave

functions of vector mesons ( $\rho, \omega, \phi$ ) are equal to that of pion's,  $\psi_V \simeq \psi_\pi$ , as they are the members of the same SU(6)-multiplet.

The total cross section  $\sigma_{\gamma p}^{tot}$  has been calculated, with the same parameters for the primary pomeron which have been found for the reactions  $pp$  and  $\pi p$ . The extra constant is the normalization parameter which determines the transition  $\gamma \rightarrow V$ ; its value is defined by  $\sigma^{tot}(\gamma p)$  at  $\sqrt{s} = W_{\gamma p} = 20$  GeV. The results of the calculation are shown in Fig. 8c, together with the available experimental data (see [42] and references therein).

In Fig. 8d we demonstrate the cross section  $\gamma p \rightarrow \rho/\omega p$  calculated under the assumption  $\sigma(\gamma p \rightarrow \rho p) = \sigma(\gamma p \rightarrow \omega p)$ . No new parameter is used comparing with the calculation of  $\sigma_{\gamma p}^{tot}$ .

**d. Effective colour screening radius  $r_{cs}^{eff}$ .** The concept of colour screening which is realized here on the basis of gluon structure of the pomeron makes it necessary to introduce, apart from the colour screening radius of a primary pomeron, the effective colour screening radius. For the pion-proton interaction, the colour screening profile factor is determined as:

$$\zeta_\pi(r, s) = N \sigma_\pi(\vec{r}_{1\perp}, \vec{r}_{2\perp}; s) = N \int d^2b dr'' \varphi_p^2(r'') \left[ 1 - \exp\left(-\frac{1}{2} \chi_{\pi p}(r, r'', b)\right) \right]. \quad (22)$$

Here  $N$  is a normalization factor which is chosen to satisfy the constraint:

$$\zeta_\pi(r \rightarrow \infty, s) = 1.$$

The physical meaning of this colour screening profile factor is simple: the pion-proton interaction  $\zeta_\pi(r, s)$  depends on the pion interquark distance, and it tends to zero with  $r \rightarrow 0$ , in line with general concept of the colour screening. After the integrations over the impact parameter  $b$  and proton coordinates  $r''$ , we have found  $\zeta_\pi(r)$  which is shown in Fig. 9 for different  $s$ . At far asymptotic energies  $\sqrt{s} \gg 10^{10}$  GeV<sup>2</sup> the effective colour screening radius tends to zero. This phenomenon comes due to the diffusion of the pomeron gluons in the impact parameter space.

For moderate and high energies a simple approximate function is useful:

$$\zeta_\pi(r, \sqrt{s} \sim 25 - 1800 \text{ GeV}) = 1 - \exp\left[-(r/r_{cs}^{eff})^n\right], \quad (23)$$

with  $n = 1.89$  and  $r_{cs}^{eff} = 0.172$  fm.

Likewise, effective colour screening radius has been defined for the proton; its numerical value practically coincides with that of pion's. It is worth noting that the effective radius  $r_{cs}^{eff}$  and colour screening radius of the primary pomeron  $r_{cs}$  are very close to each other at  $\sqrt{s} \sim 25 - 1800$  GeV.

**e. The low-energy effective pomeron.** The last point to be discussed in this section is how the performed calculations relate to the description of the diffractive processes at intermediate and moderately high energies. In the paper [12] the  $\pi p$  and  $pp$  diffractive cross sections were simultaneously described at FNAL energies, in the framework of the one-pomeron exchange with colour screening taken into account. The  $qq$ -amplitude calculated in [12] has been found to be equal to 5.5 mb. Let us consider this single

pomeron as an effective one  $\mathbf{P}_{eff}$  and compare it with analogous magnitude obtained within generalized eikonal approach developed here. The effective pomeron is actually a sum of multi-pomeron exchanges of a primary pomeron shown in Fig. 10a,b, the colour screening neglected. The summation of all the pomeron graphs of Fig. 10a,b provides the value 6 mb for  $f_{qq}^{(P_{eff})} = \sigma_{qq}^{tot}$  at  $\sqrt{s} = 24$  GeV, thus revealing a self-consistency of both approaches. It should be noted that  $\sigma_{qq}^{tot} = f_P(s_{qq}, q_{\perp}^2 = 0)$  of the primary pomeron is 9 mb at this energy and falls down to 6 mb at  $s_{qq}=10$  GeV<sup>2</sup> (see Fig. 6c). This means that multiple rescatterings are not much significant, justifying the results of the additive quark model in this region.

Calculated at different energies, this quark-pomeron amplitude  $f_{qq}^{(P_{eff})}(s, q_{\perp}^2 = 0)$  is shown in Fig. 10c; it should be emphasized that asymptotically this magnitude,  $f_{qq}^{(P_{eff})}(s, q_{\perp}^2 = 0)$ , increases as  $\ln^2 s$ .

## 4 Conclusion

In this article we have performed the description of soft diffractive processes in the  $pp(p\bar{p})$ ,  $\pi p$  and  $\gamma p$  processes within the framework of generalized eikonal approximation at the whole range of available energies, the characteristics of a soft primary pomeron have been found. Generalized eikonal approximation is a correct representation of the  $s$ -channel unitarized amplitude with respect to the leading-in- $s$  terms, provided the multi-pomeron vertices ( $\mathbf{PPP}$ ,  $\mathbf{PPPP}$ , etc) are suppressed in the  $1/N_c$  expansion ( $g_{\mathbf{PPP}} \sim 1/N_c$ ,  $g_{\mathbf{PPPP}} \sim 1/N_c^2$ , etc).

The characteristics of the soft primary pomeron occurred to be in a proximity to those of the pQCD pomeron (Lipatov's pomeron [30]). The primary pomeron is approximated by three poles in the complex plane  $j$ :

$$j = 1 - \Delta', \quad 1, \quad 1 + \Delta, \quad \text{with} \quad \Delta = 0.29 \quad \text{and} \quad \Delta' = 1.154.$$

The intercept of the leading pole is close to that of leading pole of Lipatov's pomeron. A small proper size of the soft primary pomeron, by our opinion, causes this proximity.

Mainly, the asymptotic behaviour of cross sections is determined by the leading pole with multiple rescatterings, that leads to a Froissart-type growth  $\sigma^{tot} \simeq 2\pi r_{disc}^2 \ln^2 s$ . The coefficient  $r_{disc}^2$  is of the order of  $\alpha'_{\mathbf{P}}(0)$ :  $r_{disc}^2 \simeq \alpha'_{\mathbf{P}}(0)$ . A quasi point-like structure of the primary pomeron is directly related to the small value of parameters  $r_{disc}^2 = 0.051$  mb =  $(0.071 \text{ fm})^2$  and  $r_{cs} = 0.17$  fm, that is unambiguously connected with the large effective soft gluon mass defined in the analysis of data on radiative  $J/\psi$  decay.

At asymptotic energies  $r_{cs}^{eff}(s)$  tends to 0 that is due to a large diffusion of partons in the pomeron ladder. With the energy decrease, the effective colour screening radius grows, being of the order of the primary pomeron radius in the interval  $\sqrt{s} \sim 50 - 10^{10}$  GeV. The further descent to the intermediate energies, such as  $p_{lab} \sim 50 - 100$  GeV/c, results in a decrease of the colour screening radius of the primary pomeron, that makes the effective radius much smaller too, justifying additive quark model.

The scattering amplitude which is obtained within the framework of generalized eikonal approach in the energy range  $\sqrt{s} = 25 - 1800$  GeV increases weakly, like  $s^{0.1}$ . This is just the region where the amplitude reproduces the behaviour of the KTDL-pole. The growth of  $\sigma_{\pi p}^{tot}$ ,  $\sigma_{pp}^{tot}$  and  $\sigma_{\gamma p}^{tot}$  is found to be universal that does not agree with the statement of [43] that shadowing results in process-dependent apparent intercepts for these reactions.

At intermediate energies,  $p_{lab} \simeq 50 - 100$  GeV/c, all three poles  $j < 1$  and  $j = 1$  are significant. In this region the generalized eikonal approach reproduces qualitatively the results of the quark model. The colour screening radius decreases significantly,  $r_{cs}^2(s_{qq}) \sim 5 \text{ GeV}^2 = 0.02 \pm 0.01 \text{ fm}^2$ , thus reducing the colour screening effects into amplitude. This is quite natural for intermediate energies because the colour screening, in terms of hadronic language, is due to inelastic shadowing which is small; it increases steadily with the energy growth and is stabilizing at high energies (see, for example, [27, 44] and references therein).

The performed analysis allows us to conclude that primary pomeron, which properties are close to those of Lipatov's pomeron, is a universal object for the description of soft diffractive processes in the whole interval of high energies, starting from  $\sqrt{s} \sim 25$  GeV. We would like to stress that primary pomeron with  $\Delta \simeq 0.29$ , colour screening and multiple rescatterings included, describes simultaneously the data on  $\pi p$ ,  $pp$  and  $\gamma p \rightarrow Vp$  reaction, the growth rate being nearly the same. This fact does not agree with the statement made in [43] that colour screening affects the different growth rates of cross sections for different reactions.

Concluding, we would like to underline the basic difference of the developed approach from that of Donachie–Landshoff [3, 5, 43]. In [3, 5] soft diffractive amplitudes are due to the soft pomeron exchange with  $\Delta_{soft} = 0.08$ , while a new object – hard pomeron with  $\Delta_{hard} = 0.3$  – is introduced for the vector meson electroproduction processes  $\gamma^*(Q^2)V \rightarrow VP$  [43]. The hard pomeron vertex  $\gamma^*(Q^2)V \rightarrow \text{hard pomeron}$  depends on  $Q^2$ , being rather small or equal to zero at  $Q^2 = 0$ . However, one may expect that a realization of this hypothesis in terms of quarks or hadrons needs a special dynamics: the problem is how to relate this dynamics to the vector dominance idea or, more generally, to the mechanism of the photon hadronization  $\gamma \rightarrow q\bar{q}$ .

In our model it is the primary pomeron who has  $\Delta \simeq 0.29$ , and a weak cross section growth at  $\sqrt{s} = 50 - 2000$  GeV is due to a considerable shadowing which appeared to be universal for the light hadrons and photon (within photon hadronization). One may believe that in the reaction  $\gamma^*(Q^2)V \rightarrow VP$  the shadowing effects should vanish at large  $Q^2$ , leaving the one-pomeron exchange responsible for the process at  $Q^2 \sim 10 - 20 \text{ GeV}^2$ .

## Acknowledgement

The authors are grateful to V.V. Anisovich, Ya.I. Azimov, L.N. Lipatov and M.G. Ryskin for useful discussions and comments. V.A.N. acknowledges the support of the RFBR grant N 98-02-17236.

## Appendix A. Soft pomeron and the s-channel unitarized amplitude: meson-meson elastic scattering

Here we present the formulae for the amplitudes of diffractive processes emphasizing the basic points of our approach. To illustrate the method, we consider as an example the meson-meson scattering amplitude that allows us to underline general features of the s-channel unitarization procedure. Then the formulae for the pion-nucleon and nucleon-nucleon (or nucleon-antinucleon) diffractive scattering are presented; some of them were given in [10], though without derivation.

The study of the meson-meson scattering amplitude (as well as the other diffractive amplitudes) is performed in the impact parameter space, that is suitable for the s-channel unitarization. The consideration is carried out in the following way:

- (i) First, we consider the impulse approximation diagram for the exchange of the primary pomeron **P** – the interaction of the type of Fig. 2a-b for meson- or Fig. 2e-g for proton-pomeron amplitude. For the exchange of primary pomeron, the standard eikonal unitarization is performed.
- (ii) Then, the three-reggeon **PGG** and five-reggeon **GGPGG** diagrams are considered: these diagrams are responsible for the colour screening in the primary pomeron exchange amplitude.
- (iii) As a last step, we take into account a full set of primary pomeron interactions (**P**, **PGG**, **GGP** and **GGPGG**) in the generalized eikonal approximation (Fig. 3): it provides a unitarized meson-meson scattering amplitude with a colour screening.

**a. Primary pomeron exchange and the eikonal unitarization.** Within the standard normalization, the soft-scattering amplitude of Fig. 11a reads:

$$A^{(P)}(s, q_\perp^2) = i s F_A(q_\perp^2) F_B(q_\perp^2) P(s, q_\perp^2). \quad (A.1)$$

Here  $F_A(q_\perp^2)$  and  $F_B(q_\perp^2)$  are form factors of the colliding mesons A and B ( $t \simeq -q_\perp^2$ ), and  $isP(s, q_\perp^2)$  stands for the primary pomeron propagator coupled to mesons A and B. For diffractive processes the main contribution is provided by the imaginary part of the pomeron propagator; the real part of it may be neglected, although in the calculation of scattering amplitudes the real part can be easily restored.

For the description of data with Lipatov's pomeron as a guide, the pomeron propagator is parametrized by a sum of several terms, but in this Appendix, for the simplicity sake,  $P(s, q_\perp^2)$  is treated as a one-pole term, with  $\alpha(0) = 1 + \Delta$ . Then

$$P(s, q_\perp^2) = g_A g_B s^\Delta e^{-q_\perp^2(2G + \alpha' \ln s)}. \quad (A.2)$$

Within the standard normalization, one has for the scattering amplitude  $Im A(s, 0) = s\sigma^{tot}$ , though for the calculation of multiple scatterings another amplitude normalization is more suitable, namely,  $f(s, q_\perp^2) = (is)^{-1} A(s, t)$ .

We unitarize the upper and down blocks of the diffractive amplitudes separately, and for this purpose let us cut the pomeron amplitude into two pieces as is shown in Fig. 11b:

$$f^{(P)}(s, q_\perp^2) = f_A^{(P)}(s_A, q_\perp^2) f_B^{(P)}(s_B, q_\perp^2). \quad (A.3)$$



The upper and down pieces of the whole amplitude depend on the energies squared  $s_A$  and  $s_B$ , which obey the equality  $sm_0^2 = s_A s_B$  (below  $m_0 = 1$  GeV is chosen). Consider the upper block in details; it is equal to:

$$f_A^{(P)}(s_A, q_\perp^2) = F_A(q_\perp^2) g_A s_A^\Delta e^{-(G+\alpha' \ln s_A) q_\perp^2}. \quad (A.4)$$

The amplitude  $f_A^{(P)}(s_A, q_\perp^2)$  represented as an integral in the impact parameter space reads:

$$f_A^{(P)}(s_A, q_\perp^2) = \int d^2 b_A e^{i\vec{q}_\perp \vec{b}_A} \int d^2 r_\perp \varphi_A^2(\vec{r}_\perp) \rho_A(\vec{b}_A - \vec{r}_\perp, s_A). \quad (A.5)$$

Here  $\rho_A(\vec{b}_A, s_A)$  is the pomeron propagator coupled to meson  $A$ ,

$$\rho_A(\vec{b}_A, s_A) = \int \frac{d^2 q_\perp}{(2\pi)^2} e^{-i\vec{q}_\perp \vec{b}_A} g_A s_A^\Delta e^{-(G+\alpha' \ln s_A) q_\perp^2}, \quad (A.6)$$

while  $\varphi_A^2(\vec{r}_\perp)$  is the Fourier tranform of the pion form factor:

$$\varphi_A^2(\vec{r}_\perp) = \int \frac{d^2 q_\perp}{(2\pi)^2} e^{i\vec{q}_\perp \vec{r}_\perp} F_A(q_\perp^2). \quad (A.7)$$

With this definition, the density  $\varphi_A^2(\vec{r}_\perp)$  in the impact parameter space is invariant in respect to the boost along the  $z$ -axis.

The down block of Fig. 11b is treated similarly, so one has:

$$f_B^{(P)}(s_B, q_\perp^2) = \int d^2 b_B e^{-i\vec{q}_\perp \vec{b}_B} \int d^2 r'_\perp \varphi_B^2(\vec{r}'_\perp) \rho_B(\vec{b}_B - \vec{r}'_\perp, s_B). \quad (A.8)$$

Here we take into account that  $\vec{q}_\perp$  is the incoming momentum for the lower block, while for the upper block it is the outgoing one.

The one-pomeron exchange amplitude of Fig. 11a, after replacing  $\vec{r}_\perp \rightarrow \vec{r}$  and  $\vec{r}'_\perp \rightarrow \vec{r}'$ , reads:

$$f^{(P)}(s, q_\perp^2) = \int d^2 b e^{i\vec{q}_\perp \vec{b}} \int d^2 r \varphi_A^2(\vec{r}) d\vec{r}' \varphi_B^2(\vec{r}') \chi(\vec{r}, \vec{r}', b), \quad (A.9)$$

where

$$\chi(\vec{r}, \vec{r}', b) = \int d^2 b_A d^2 b_B \delta(\vec{b} - \vec{b}_A + \vec{b}_B) \rho_A(\vec{b}_A - \vec{r}_\perp, s_A) \rho_B(\vec{b}_B - \vec{r}'_\perp, s_B). \quad (A.10)$$

Here  $\chi(\vec{r}, \vec{r}', b)$  is the eikonal profile function, which takes account of all the multi-pomeron exchanges in a standard way (for example, see [45, 46]). The amplitude with  $n$ -pomeron exchanges shown in Fig. 3 ( $n \geq 1$ ) is equal to:

$$f^{(PP\dots P)}(s, q_\perp^2) = \int d^2 b e^{i\vec{q}_\perp \vec{b}} \int d\vec{r} \varphi_A^2(\vec{r}) d\vec{r}' \varphi_B^2(\vec{r}') \frac{2}{n!} \left( -\frac{1}{2} \chi(\vec{r}, \vec{r}', b) \right)^n. \quad (A.11)$$

So, the scattering amplitude  $AB \rightarrow AB$  with a full set of the primary pomeron exchanges reads:

$$f_{AB \rightarrow AB}(s, q_\perp^2) = 2 \int d^2 b e^{i\vec{q}_\perp \vec{b}} \int d\vec{r} \varphi_A^2(\vec{r}) d\vec{r}' \varphi_B^2(\vec{r}') \left( 1 - e^{-\frac{1}{2} \chi(\vec{r}, \vec{r}', b)} \right). \quad (A.12)$$

The normalization condition is  $f_{AB \rightarrow AB}(s, 0) = \sigma_{AB}^{tot}$ .

The equation (A.12) specifies neither the type of constituents responsible for the pomeron interaction nor the characteristics of the constituent distributions,  $\varphi_A^2(\vec{r})$  and  $\varphi_B^2(\vec{r})$ , measured by the pomeron. This specification will be done below in terms of the quark model.

**b. Colliding meson as loosely bound  $q\bar{q}$  system.** Here the interpretation of the distribution functions  $\varphi_A^2(\vec{r})$  and  $\varphi_B^2(\vec{r})$  is given in terms of the quark model. For this purpose, consider the scattering process in the laboratory frame, initial meson  $A$  being at rest. The form factor of the meson  $A$  is determined by the standard non-relativistic quark model expression:

$$F_A(q_\perp) = \int \frac{d^3k}{(2\pi)^3} \psi_A(k) \psi_A(|\vec{k} + \frac{1}{2}\vec{q}_\perp|) = \int d^3r_{q\bar{q}} \phi_A^2(r_{q\bar{q}}) e^{\frac{i}{2}\vec{r}_{q\bar{q}}\vec{q}_\perp}, \quad (A.13)$$

where  $\vec{k}$  is relative quark-antiquark momentum,  $\vec{k} = \frac{1}{2}(\vec{k}_q - \vec{k}_{\bar{q}})$ , and  $\vec{r}_{q\bar{q}}$  is interquark distance,  $\vec{r}_{q\bar{q}} = \vec{r}_q - \vec{r}_{\bar{q}}$ . The integration over  $dr_{q\bar{q}z}$  introduces the quark density in the  $\vec{r}_{q\bar{q}\perp}$ -space:

$$\varphi_A^2(\vec{r}_\perp) = \int dr_{q\bar{q}z} \phi_A^2(r_{q\bar{q}}). \quad (A.14)$$

One more specification is suitable here, namely, an explicit integration over quark and antiquark coordinates  $\vec{r}_{q\perp}$  and  $\vec{r}_{\bar{q}\perp}$ :

$$F_A(q_\perp) = \int d^2\vec{r}_{q\perp} d^2\vec{r}_{\bar{q}\perp} \delta(\vec{r}_{q\perp} + \vec{r}_{\bar{q}\perp}) \Phi_A^2(\vec{r}_{q\perp}, \vec{r}_{\bar{q}\perp}) e^{i\vec{r}_{q\perp}\vec{q}_\perp}, \quad (A.15)$$

where  $\Phi_A^2(\vec{r}_{q\perp}, \vec{r}_{\bar{q}\perp}) = \varphi_A^2(\frac{1}{2}|\vec{r}_{q\perp} - \vec{r}_{\bar{q}\perp}|)$ . Then, for the case of a pomeron coupled to one quark of the meson  $A$  (Fig. 2a-b), the amplitude reads:

$$f_{Aq}^{(P)}(s_A, q_\perp^2) = \int d^2b_A e^{i\vec{q}_\perp \vec{b}_A} \int d^2\vec{r}_{q\perp} d^2\vec{r}_{\bar{q}\perp} \delta(\vec{r}_{q\perp} + \vec{r}_{\bar{q}\perp}) \Phi_A^2(\vec{r}_{q\perp}, \vec{r}_{\bar{q}\perp}) \rho_{Aq}(\vec{b}_A - r_{q\perp}, s_{Aq}), \quad (A.16)$$

$$\rho_{Aq}(\vec{b}_A, s_{Aq}) = \int \frac{d^2q_\perp}{(2\pi)^2} e^{-i\vec{q}_\perp \vec{b}_A} g_{Aq} s_{Aq}^\Delta e^{-(G+\alpha' \ln s_{Aq})q_\perp^2},$$

In (A.16) we take into consideration that the quarks of the mesons  $A$  and  $B$  share the invariant energy squared:

$$s_A = s_{Aq} + s_{A\bar{q}}, \quad s_B = s_{Bq} + s_{B\bar{q}}. \quad (A.17)$$

For mesons with equal quark masses  $m_q = m_{\bar{q}}$ ,

$$s_{Aq} \simeq s_{A\bar{q}} \simeq \frac{1}{2}s_A, \quad \text{and} \quad s_{Bq} \simeq s_{B\bar{q}} \simeq \frac{1}{2}s_B. \quad (A.18)$$

The interaction of meson  $B$  with the primary pomeron is treated in the same way, implying the quark density in the impact parameter space be invariant under the boost along the  $z$ -axis:

$$f_{Bq}^{(P)}(s_B, q_\perp^2) = \int d^2b_B e^{-i\vec{q}_\perp \vec{b}_B} \int d^2\vec{r}_{q\perp} d^2\vec{r}_{\bar{q}\perp} \delta(\vec{r}_{q\perp} + \vec{r}_{\bar{q}\perp}) \Phi_B^2(\vec{r}_{q\perp}, \vec{r}_{\bar{q}\perp}) \rho_{Bq}(\vec{b}_B - r_{q\perp}, s_{Bq}), \quad (A.19)$$

$$\rho_{Bq}(\vec{b}_B, s_{Bq}) = \int \frac{d^2 q_\perp}{(2\pi)^2} e^{i\vec{q}_\perp \vec{b}_B} g_{Bq} s_{Bq}^\Delta e^{-(G+\alpha' \ln s_{Bq})q_\perp^2},$$

To take account of the pomeron exchanges between different quarks (Fig. 2c), one should make a substitution in (A.16) and (A.19) as follows:

$$\begin{aligned} \rho_{Aq}(\vec{b}_A - \vec{r}'_{q\perp}, s_{Aq}) &\rightarrow \rho_{Aq}(\vec{b}_A - \vec{r}_{q\perp}, s_{Aq}) + \rho_{A\bar{q}}(\vec{b}_A - \vec{r}_{\bar{q}\perp}, s_{A\bar{q}}) \equiv \rho_A^{(without\ cs)}(\vec{b}_A, \vec{r}, s_A), \\ \rho_{Bq}(\vec{b}_B - \vec{r}'_{q\perp}, s_{Bq}) &\rightarrow \rho_{Bq}(\vec{b}_B - \vec{r}'_{q\perp}, s_{Bq}) + \rho_{B\bar{q}}(\vec{b}_B - \vec{r}'_{\bar{q}\perp}, s_{B\bar{q}}) \equiv \rho_B^{(without\ cs)}(\vec{b}_B, \vec{r}', s_B). \end{aligned} \quad (A.20)$$

Using (A.20), one can apply the formulae (A.10)–(A.12) to the calculation of the scattering amplitude for  $q\bar{q}$  mesons  $A$  and  $B$ , with compact notations for quark variables:

$$\begin{aligned} d^2 \vec{r}_{q\perp} d^2 \vec{r}_{\bar{q}\perp} \delta(\vec{r}_{q\perp} + \vec{r}_{\bar{q}\perp}) \Phi_A^2(\vec{r}_{q\perp}, \vec{r}_{\bar{q}\perp}) &\equiv d^2 r \varphi_A^2(\vec{r}), \\ d^2 \vec{r}'_{q\perp} d^2 \vec{r}'_{\bar{q}\perp} \delta(\vec{r}'_{q\perp} + \vec{r}'_{\bar{q}\perp}) \Phi_B^2(\vec{r}'_{q\perp}, \vec{r}'_{\bar{q}\perp}) &\equiv d^2 r' \varphi_B^2(\vec{r}'). \end{aligned} \quad (A.21)$$

This procedure provides us with a unitarized scattering amplitude, but so far the colour screening has not been taken into consideration.

**c. Colour screening effects for the scattering of loosely bound systems.** In the Lipatov's pomeron picture, the colour screening is due to the two types of coupling of reggeized gluons to meson quarks, either with the same quark (antiquark) (Fig. 12a,b) or with both of them (Fig. 12c).

Let the meson  $A$  be at rest and  $s_A$  rather large,  $s_A \sim s$ , see Fig. 12c; then compare these two types of meson–pomeron vertices. The amplitude related to the sum of the Fig. 12a-b diagrams is considered in more details in Appendix B; here we would like to illustrate the scheme of how the colour screening emerges for a loosely bound meson. The amplitude corresponding to diagrams of Fig. 12a-c is equal to

$$\begin{aligned} f_A^{(\mathbf{P}+\mathbf{P}+\mathbf{P}\mathbf{G}\mathbf{G})}(q_\perp^2) &= 2 \int \frac{d^3 \kappa}{(2\pi)^3} \int \frac{d^3 k}{(2\pi)^3} \left[ \psi_A(k) \psi_A(|\vec{k} + \frac{1}{2} \vec{q}_\perp|) - \psi_A(k) \psi_A(|\vec{k} + \vec{\kappa}_\perp|) \right] \\ &\quad \times a_{\mathbf{P}\mathbf{G}\mathbf{G}} \left( (\vec{\kappa}_\perp + \frac{1}{2} \vec{q}_\perp)^2, (-\vec{\kappa}_\perp + \frac{1}{2} \vec{q}_\perp)^2, \kappa_z \right). \end{aligned} \quad (A.22)$$

The term proportional to  $\psi_A(k) \psi_A(|\vec{k} + \frac{1}{2} \vec{q}_\perp|)$  is the impulse approximation contribution, while the second one in the integrand (A.22) is due to the triple-reggeon diagram  $a_{\mathbf{P}\mathbf{G}\mathbf{G}}$ , which itself is shown in Fig. 12c. It depends on  $s_A$  and  $\kappa_z = m_0 M^2 / s_A$ , where  $M^2$  is invariant energy squared carried by the pomeron (see Appendix B for details):

$$a_{\mathbf{P}\mathbf{G}\mathbf{G}} \left( (\vec{\kappa}_\perp + \frac{1}{2} \vec{q}_\perp)^2, (-\vec{\kappa}_\perp + \frac{1}{2} \vec{q}_\perp)^2, \kappa_z \right) \simeq R s_A^\Delta \kappa_z^{\alpha(0)-2\alpha_G(0)}. \quad (A.23)$$

Here  $\alpha_{\mathbf{P}}(0)$  and  $\alpha_{\mathbf{G}}(0)$  are the pomeron and reggeized gluon intercepts:  $\alpha(0) = 1 + \Delta$  and  $\alpha_{\mathbf{G}}(0) \simeq 1$ . The coefficient  $R$  in the r.h.s. (A.23) is a function of  $q_\perp^2$ ,  $(\vec{\kappa}_\perp + \frac{1}{2} \vec{q}_\perp)^2$  and  $(-\vec{\kappa}_\perp + \frac{1}{2} \vec{q}_\perp)^2$ . Taking this coefficient in the exponential form, as is usual for the reggeon exchange amplitudes, one obtains:

$$R \sim e^{-\beta q_\perp^2} e^{-\gamma(\vec{\kappa}_\perp + \frac{1}{2} \vec{q}_\perp)^2} e^{-\gamma(-\vec{\kappa}_\perp + \frac{1}{2} \vec{q}_\perp)^2} = e^{-(\beta + \frac{1}{2}\gamma)q_\perp^2} e^{-2\gamma\kappa_\perp^2}. \quad (A.24)$$

After having integrated over  $\vec{k} = \frac{1}{2}(\vec{k}_q - \vec{k}_{\bar{q}})$ , one has:

$$f_A^{(P+P+PGG)}(q_\perp^2) = 2F_A(q_\perp^2) \int \frac{d^3\kappa}{(2\pi)^3} a_{\mathbf{P}\mathbf{G}\mathbf{G}} \left( (\vec{\kappa}_\perp + \frac{1}{2}\vec{q}_\perp)^2, (-\vec{\kappa}_\perp + \frac{1}{2}\vec{q}_\perp)^2, \kappa_z \right) \\ - 2 \int \frac{d^3\kappa}{(2\pi)^3} F_A(\kappa^2) a_{\mathbf{P}\mathbf{G}\mathbf{G}} \left( (\vec{\kappa}_\perp + \frac{1}{2}\vec{q}_\perp)^2, (-\vec{\kappa}_\perp + \frac{1}{2}\vec{q}_\perp)^2, \kappa_z \right). \quad (\text{A.25})$$

This expression can be compared with (A.4) written for the impulse approximation amplitude; the comparison provides

$$g_A s_A^\Delta e^{-(G+\alpha' \ln s_A) q_\perp^2} = 2 \int \frac{d^3\kappa}{(2\pi)^3} a_{\mathbf{P}\mathbf{G}\mathbf{G}} \left( (\vec{\kappa}_\perp + \frac{1}{2}\vec{q}_\perp)^2, (-\vec{\kappa}_\perp + \frac{1}{2}\vec{q}_\perp)^2, \kappa_z \right). \quad (\text{A.26})$$

Equation (A.26) allows us to see the colour screening in its explicit form: for a point-like meson  $A$  one has  $F_A = 1$ , and the amplitude (A.25) equals to zero. Still, more suitable for this purpose is the coordinate representation. The three-reggeon amplitude  $a_{\mathbf{P}\mathbf{G}\mathbf{G}}$  depends on  $\vec{r}_{g1}$  and  $\vec{r}_{g2}$  which are the gluon coordinates in the impact parameter space:

$$a_{\mathbf{P}\mathbf{G}\mathbf{G}}(\kappa_{1\perp}^2, \kappa_{2\perp}^2, \kappa_z) = \int d^2r_{g1} d^2r_{g2} a_{\mathbf{P}\mathbf{G}\mathbf{G}}^{(\text{coordinate})}(r_{g1}, r_{g2}, \kappa_z) e^{i(\vec{r}_{g1}\vec{\kappa}_{1\perp} + \vec{r}_{g2}\vec{\kappa}_{2\perp})}. \quad (\text{A.27})$$

Then (A.25) reads:

$$f_A^{(\mathbf{P}+\mathbf{P}+\mathbf{P}\mathbf{G}\mathbf{G})}(q_\perp^2) = 2 \int \frac{d\kappa_z}{2\pi} \int d^3r_{q\bar{q}} \int d^2r_{g1} d^2r_{g2} \phi_A^2(r_{q\bar{q}}) a_{\mathbf{P}\mathbf{G}\mathbf{G}}^{(\text{coordinate})}(r_{g1}, r_{g2}, \kappa_z) \\ \times \left[ e^{\frac{i}{2}(\vec{r}_{q\bar{q}\perp} + \vec{r}_{g1} + \vec{r}_{g2})\vec{q}_\perp} \delta(\vec{r}_{g1} - \vec{r}_{g2}) - e^{ir_{q\bar{q}z}\kappa_z} e^{\frac{i}{2}(\vec{r}_{g1} + \vec{r}_{g2})\vec{q}_\perp} \delta(\vec{r}_{g1} - \vec{r}_{g2} - \vec{r}_{q\bar{q}\perp}) \right]. \quad (\text{A.28})$$

The integrand in (A.28) tends to zero with  $|\vec{r}_{q\bar{q}\perp}| \rightarrow 0$  and  $r_{q\bar{q}z} \rightarrow 0$ : this is a manifestation of the colour screening. Moreover, the colour screening reveals itself when, after the integration over  $r_{q\bar{q}z}$ , the expression  $|\vec{r}_{q\bar{q}\perp}|$  tends to zero. The matter is that the dominant contribution to the integral (A.28) is given by the region  $\kappa_z \sim 0$ . Hence

$$|r_{q\bar{q}z}\kappa_z| \ll 1. \quad (\text{A.29})$$

So, with a sufficiently good accuracy, one can substitute in (A.28)  $\exp(ir_{q\bar{q}z}\kappa_z) \rightarrow 1$  (for more details see Appendix B). As a result, using the variables  $\vec{b}_A = \frac{1}{2}(\vec{r}_{g1} + \vec{r}_{g2})$  and  $\vec{r}_{gg} = \vec{r}_{g1} - \vec{r}_{g2}$ , we have

$$f_A^{(\mathbf{P}+\mathbf{P}+\mathbf{P}\mathbf{G}\mathbf{G})}(q_\perp^2) = \\ 2 \int \frac{d\kappa_z}{2\pi} \int d^2r_{q\bar{q}\perp} \int d^2b_A \varphi_A^2(r_{q\bar{q}\perp}) a_{\mathbf{P}\mathbf{G}\mathbf{G}}^{(\text{coordinate})}(b_A^2, b_A^2, \kappa_z) e^{i(\vec{b}_A + \frac{1}{2}\vec{r}_{q\bar{q}\perp})\vec{q}_\perp} \\ - 2 \int \frac{d\kappa_z}{2\pi} \int d^2r_{q\bar{q}\perp} \int d^2b_A \varphi_A^2(r_{q\bar{q}\perp}) a_{\mathbf{P}\mathbf{G}\mathbf{G}}^{(\text{coordinate})}((\vec{b}_A - \frac{1}{2}\vec{r}_{q\bar{q}\perp})^2, (\vec{b}_A + \frac{1}{2}\vec{r}_{q\bar{q}\perp})^2, \kappa_z) e^{i\vec{b}_A\vec{q}_\perp}. \quad (\text{A.30})$$

Finally, with the re-definition in the first term  $\vec{b}_A + \frac{1}{2}\vec{r}_{q\bar{q}\perp} \rightarrow \vec{b}_A$ , we have:

$$f_A^{(\mathbf{P}+\mathbf{P}+\mathbf{PGG})}(q_\perp^2) = 2 \int d^2b e^{i\vec{b}_A \vec{q}_\perp} \int d^2r_{q\bar{q}\perp} \varphi_A^2(r_{q\bar{q}\perp}) \int \frac{d\kappa_z}{2\pi} a_{\mathbf{PGG}}^{(\text{coordinate})} \left( (\vec{b}_A - \frac{1}{2}\vec{r}_{q\bar{q}\perp})^2, (\vec{b}_A - \frac{1}{2}\vec{r}_{q\bar{q}\perp})^2, \kappa_z \right) - 2 \int d^2b_A e^{i\vec{b}_A \vec{q}_\perp} \cdot \int d^2r_{q\bar{q}\perp} \varphi_A^2(r_{q\bar{q}\perp}) \int \frac{d\kappa_z}{2\pi} a_{\mathbf{PGG}}^{(\text{coordinate})} \left( (\vec{b}_A - \frac{1}{2}\vec{r}_{q\bar{q}\perp})^2, (\vec{b}_A + \frac{1}{2}\vec{r}_{q\bar{q}\perp})^2, \kappa_z \right). \quad (\text{A.31})$$

In our notations

$$\rho_A(\vec{b}_A, s_A) = \int \frac{d\kappa_z}{2\pi} a_{\mathbf{PGG}}^{(\text{coordinate})}(b_A^2, b_A^2, \kappa_z), \quad (\text{A.32})$$

then with the exponential parametrization (A.23) one has:

$$\int \frac{d\kappa_z}{2\pi} a_{\mathbf{PGG}}^{(\text{coordinate})} \left( (\vec{b}_A - \frac{1}{2}\vec{r}_{q\bar{q}\perp})^2, (\vec{b}_A + \frac{1}{2}\vec{r}_{q\bar{q}\perp})^2, \kappa_z \right) = \rho_A(\vec{b}, s_A) \exp \left( -\frac{r_{q\bar{q}\perp}^2}{r_{cs}^2} \right). \quad (\text{A.33})$$

Using the variables given in (A.15)–(A.16), we have

$$f_A^{(P+P+PGG)}(q_\perp^2) = 2 \int d^2b e^{i\vec{b}_A \vec{q}_\perp} \int d^2\vec{r}_{q\perp} d^2\vec{r}_{\bar{q}\perp} \delta(\vec{r}_{q\perp} + \vec{r}_{\bar{q}\perp}) \Phi_A^2(\vec{r}_{q\perp}, \vec{r}_{\bar{q}\perp}) \rho_A(\vec{b}_A, \vec{r}, s_A), \quad (\text{A.34})$$

with the colour screening term included into the primary pomeron amplitude:

$$\rho_A(\vec{b}_A, \vec{r}, s_A) = \rho_A(\vec{b}_A - \vec{r}_{q\perp}, s_A) + \rho_A(\vec{b}_A - \vec{r}_{\bar{q}\perp}, s_A) - 2\rho_A(\vec{b} - \frac{\vec{r}_{q\perp} + \vec{r}_{\bar{q}\perp}}{2}, s_A) e^{-\frac{(\vec{r}_{q\perp} - \vec{r}_{\bar{q}\perp})^2}{4r_{cs}^2}}. \quad (\text{A.35})$$

This amplitude should be compared with (A.20), written without colour screening term.

Likewise, the amplitude  $f_B^{(\mathbf{P}+\mathbf{P}+\mathbf{PGG})}(q_\perp^2)$  is written, with the replacements  $A \rightarrow B$  and  $\vec{q}_\perp \rightarrow -\vec{q}_\perp$ .

The full amplitude with the  $s$ -channel unitarization is given by (A.12) with the profile function determined as follows:

$$\chi(\vec{r}, \vec{r}', b) = \int d^2b_A d^2b_B \delta(\vec{b} - \vec{b}_A + \vec{b}_B) \rho_A(\vec{b}_A, \vec{r}, s_A) \rho_B(\vec{b}_B, \vec{r}', s_B). \quad (\text{A.36})$$

## Appendix B. Meson–pomeron coupling

Here we calculate the coupling of the three-reggeon amplitude  $\mathbf{PGG}$  to meson. The meson is treated as a loosely bound  $q\bar{q}$  system.

**a. Three-reggeon amplitude  $a_{\mathbf{PGG}}$ .** This amplitude depends on three invariant energies squared which are rather large,  $s$ ,  $s'$  and  $M^2$ , and three momentum transfers,  $t_1$ ,  $t_2$  and  $q^2$ , which are small (see Fig. 12c). With standard normalization, the amplitude  $\mathbf{PGG}$  has the form [45, 47]:

$$A_{\mathbf{PGG}} = R(t_1, t_2, q^2) e^{i\frac{\pi}{2}\alpha_{\mathbf{P}}(q^2)} (M^2)^{\alpha_{\mathbf{P}}(q^2)} \left( \frac{s}{M^2} \right)^{\alpha_{\mathbf{G}}(t_1)} \left( \frac{s'}{M^2} \right)^{\alpha_{\mathbf{G}}(t_2)}. \quad (\text{B.1})$$

At  $\alpha_{\mathbf{P}}(0) \simeq 1$ , the imaginary part of the pomeron amplitude provides a dominant contribution. Then, using an exponential parametrisation for the momentum transfer dependence, one has:

$$A_{\mathbf{P}\mathbf{G}\mathbf{G}} \simeq i R e^{-\beta(\kappa_{1\perp}^2 + \kappa_{2\perp}^2) - \gamma q_{\perp}^2} (s s')^{\frac{\alpha_{\mathbf{P}}(0)}{2}} (y y')^{\frac{\alpha_{\mathbf{P}}(0)}{2} - \alpha_{\mathbf{G}}(0)}. \quad (B.2)$$

Here  $t_i \simeq -\kappa_{i\perp}^2$  and  $q^2 \simeq -q_{\perp}^2$ . The following notations are used:  $y = M^2/s$  and  $y' = M^2/s'$ . For the three-reggeon amplitude,  $y$  and  $y'$  are small, because  $s' \sim s \ll M^2$ . The coefficients  $\beta$  and  $\gamma$  include the weak (logarithmic) dependence on  $s$ ,  $s'$  and  $M^2$  that originates from the standard expansion of reggeon trajectories:  $\alpha_{\mathbf{P}}(q^2) \simeq \alpha_{\mathbf{P}}(0) - \alpha'_{\mathbf{P}} q_{\perp}^2$  and  $\alpha_{\mathbf{G}}(t) \simeq \alpha_{\mathbf{G}}(0) - \alpha'_{\mathbf{G}} \kappa_{\perp}^2$ .

Imposing  $s' = s$ , the amplitude used in calculations is as follows:

$$a_{\mathbf{P}\mathbf{G}\mathbf{G}} = \frac{1}{i s} A_{\mathbf{P}\mathbf{G}\mathbf{G}} \simeq R e^{-\beta(\kappa_{1\perp}^2 + \kappa_{2\perp}^2) - \gamma q_{\perp}^2} s^{\Delta} y^{\alpha_{\mathbf{P}}(0) - 2\alpha_{\mathbf{G}}(0)}. \quad (B.3)$$

Being a real function, the amplitude  $a_{\mathbf{P}\mathbf{G}\mathbf{G}}$  is related to cutting of Fig. 12d–diagram along the pomeron line. This means that  $s a_{\mathbf{P}\mathbf{G}\mathbf{G}}$  given by (B.3) is a discontinuity of  $A_{\mathbf{P}\mathbf{G}\mathbf{G}}$  across the  $M^2$ -cut:

$$a_{\mathbf{P}\mathbf{G}\mathbf{G}} \simeq \frac{1}{s} \text{disc}_{M^2} A_{\mathbf{P}\mathbf{G}\mathbf{G}}. \quad (B.4)$$

Therefore,  $A_{\mathbf{P}\mathbf{G}\mathbf{G}}$  can be represented as a dispersion integral over  $M^2$ ,  $s a_{\mathbf{P}\mathbf{G}\mathbf{G}}$  being an integrand.

**b. Two-gluon interaction with a quark.** The interaction diagram is shown in Fig. 12a: reggeized gluons interact with the same quark. The meson A is treated in the rest frame, therefore, a non-relativistic quark propagator technique is appropriate here:  $(m^2 - k^2)^{-1} \simeq (-2mE + \vec{k}^2 - i0)^{-1}$ , where  $E = k_0 - m$ . The amplitude of the Fig. 12a–diagram is:

$$\begin{aligned} A^{(P)}(s, q_{\perp}^2) &= \int \frac{dE_{\bar{q}} d^3 k_{\bar{q}}}{i(2\pi)^4} \int \frac{d^4 \kappa_1}{i(2\pi)^4} \frac{G_A}{-2mE_q + \vec{k}_q^2 - i0} \cdot \frac{1}{-2mE_{\bar{q}} + \vec{k}_{\bar{q}}^2 - i0} \\ &\times \frac{1}{-2mE_q'' + \vec{k}_q''^2 - i0} \cdot \frac{G_A}{-2mE_q' + \vec{k}_q'^2 - i0} \int \frac{dM^2}{\pi} \cdot \frac{g^2 \tilde{a}(\kappa_1^2, \kappa_2^2, M^2)}{M^2 - (P_B - \kappa_1)^2 - i0}. \end{aligned} \quad (B.5)$$

The notations of momenta are shown in Fig. 12a. The vertex function  $G_A$  depends on the relative quark–antiquark momentum, namely,  $(k_q - k_{\bar{q}})^2 \simeq -(\vec{k}_q - \vec{k}_{\bar{q}})^2$  for the incoming meson vertex and  $(\vec{k}_q' - \vec{k}_{\bar{q}}')^2 \simeq -(\vec{k}_q'' - \vec{k}_{\bar{q}}'')^2$  for outgoing one. The three-reggeon amplitude  $\mathbf{P}\mathbf{G}\mathbf{G}$  is written as a dispersion integral over  $M^2$ ,  $g$  being the quark-gluon coupling. Three integrations in (B.1) are easy to perform. When integrating over  $E_{\bar{q}}$  and  $\kappa_0$ , the substitutions are made:

$$(-2mE_{\bar{q}} + \vec{k}_{\bar{q}}^2 - i0)^{-1} \rightarrow \frac{i\pi}{m} \delta \left( E_{\bar{q}} - \frac{\vec{k}_{\bar{q}}^2}{2m} \right),$$

$$(-2mE_q'' + \vec{k}_q'^2 - i0)^{-1} \rightarrow \frac{i\pi}{m} \delta \left( \kappa_{10} - \epsilon - \frac{(\vec{k}_q^2 + \vec{\kappa}_1)^2}{2m} - \frac{\vec{k}_q^2}{2m^2} \right). \quad (B.6)$$

where  $\epsilon = 2m - \mu_A$ . The real part of the three-reggeon diagram  $A_{\mathbf{PGG}}$  is small, see (B.4). Therefore, in the dispersion integral over  $M^2$  the main contribution comes from the half-residue:

$$(M^2 - (P_B - \kappa_1)^2 - i0)^{-1} \rightarrow i\pi \delta(M^2 + 2p_B \kappa_{1z}), \quad (B.7)$$

$p_B$  being a large momentum carried by a particle  $B$  along the  $z$ -axis:  $P_B = (P_{B0}, \vec{P}_\perp, P_{Bz}) = (p_B + \mu_B^2/(2p_B), 0, -p_B)$  and  $s \simeq 2p_B \mu_A$ . The terms of the order of  $m/p_B$  are neglected.

After integrating over  $E_{\bar{q}}$ ,  $\kappa_{10}$  and  $M^2$ , we obtain:

$$A^{(P)}(s, q_\perp^2) = \int \frac{d^3 k_{q\bar{q}}}{(2\pi)^3} \psi_A(k_{q\bar{q}}) \psi_A(|\vec{k}_{q\bar{q}} + \frac{1}{2}\vec{q}_\perp|) \int \frac{d^3 \kappa_1}{(2\pi)^3} \frac{i}{2m} g^2 \tilde{a}(\kappa_{1\perp}^2, \kappa_{2\perp}^2, -2p_B \kappa_{1z}), \quad (B.8)$$

where

$$\psi_A(k_{q\bar{q}}) = \frac{G_A}{2\sqrt{2m}(m\epsilon + \vec{k}_{q\bar{q}}^2)}. \quad (B.9)$$

For the three-reggeon diagram of Fig. 12a the following constraint is imposed:  $s \gg M^2 = -2p_B \kappa_{1z} \gg m^2$ . This means that  $\kappa_{1z}$  is negative and small,  $|\kappa_{1z}| \ll \mu_A$ .

Comparing (B.8) with the first term of the right-hand side of (A.22) gives us the following equality:

$$g^2 \tilde{a}(\kappa_{1\perp}^2, \kappa_{2\perp}^2, 2p_B \kappa_z) = 2m s a_{\mathbf{PGG}}(\kappa_{1\perp}^2, \kappa_{2\perp}^2, \kappa_z) F_B(q_\perp^2), \quad (B.10)$$

where  $\kappa_{1z} = -\kappa_z$ . Here we take into account that the form factor of meson B,  $F_B(q_\perp^2)$ , enters the lower block of Fig. 12a.

The expression for the antiquark-pomeron interaction is identical to that of the quark, for the integrand (B.8) is invariant with respect to the replacement  $\vec{k}_q \rightarrow \vec{k}_{\bar{q}}$  and  $g \rightarrow -g$ .

**c. The interaction of gluons with quark and antiquark.** The graphical representation of the amplitude is shown in Fig. 12b. The amplitude reads:

$$\begin{aligned} A^{(\mathbf{PGG})}(s, q_\perp^2) &= \int \frac{dE_{\bar{q}} d^3 k_{\bar{q}}}{i(2\pi)^4} \int \frac{d^4 \kappa_1}{i(2\pi)^4} \frac{G_A}{-2mE_{\bar{q}} + \vec{k}_{\bar{q}}^2 - i0} \cdot \frac{1}{-2mE_q + \vec{k}_q^2 - i0} \\ &\times \frac{1}{-2mE'_q + \vec{k}_q'^2 - i0} \cdot \frac{G_A}{-2mE'_q + \vec{k}_q'^2 - i0} \int \frac{dM^2}{\pi} \cdot \frac{(-g^2) \tilde{a}(\kappa_{1\perp}^2, \kappa_{\bar{q}}^2, M^2)}{M^2 - (P_B - \kappa_1)^2 - i0}. \end{aligned} \quad (B.11)$$

The factor  $-g^2$  in the r.h.s. of (B.11) is due to the interaction of gluons with quark and antiquark. The integrations over  $E_{\bar{q}}$  and  $E'_q$  are equivalent to the replacements:

$$(-2mE_{\bar{q}} + \vec{k}_{\bar{q}}^2)^{-1} \rightarrow \frac{i\pi}{m} \delta \left( E_{\bar{q}} - \frac{\vec{k}_{\bar{q}}^2}{2m} \right),$$

$$(-2mE'_q + \vec{k}_q'^2)^{-1} \rightarrow \frac{i\pi}{m} \delta \left( \epsilon + \frac{\vec{k}_q'^2}{2m^2} + \frac{(\vec{k}_q'^2 + \vec{\kappa}_1)^2}{2m} - \kappa_{10} \right), \quad (B.12)$$

and the integration over  $M^2$  is eliminated due to the replacement (B.7). We have

$$A^{(\text{PGG})}(s, q_\perp^2) = - \int \frac{d^3 k_{\bar{q}}}{(2\pi)^3} \int \frac{d^3 \kappa}{(2\pi)^3} \frac{G_A}{2\sqrt{2m}(\epsilon + \vec{k}_{q\bar{q}}^2)} \cdot \frac{G_A}{2\sqrt{2m}(\epsilon + (\vec{k}_{q\bar{q}} + \vec{\kappa})^2)} \\ \times \frac{i}{m} g^2 \tilde{a}(\kappa_{1\perp}^2, \kappa_{2\perp}^2, 2p_B \kappa_z). \quad (B.13)$$

Implying (B.9) and (B.10), one has the second term in (A.22).

Here, as for the diagram of Fig. 12a, the three-regeon amplitude determines the integration region over  $\kappa_z$ : the constraint  $s \gg M^2$  means that  $\kappa_z$  is small in the hadronic scale. This justifies the approximation given by (A.29).

## Appendix C. Pomeron–meson interaction in terms of the light–cone variables

Here, in terms of the light–cone variables, we calculate the diagrams shown in Fig. 12a,b.

**a. The pomeron interacting with a quark, Fig. 12a.** This diagram written as a spectral integral over  $q\bar{q}$  invariant mass reads:

$$A^{(P)}(s, q_\perp^2) = \int_{4m^2}^\infty \frac{dM_{q\bar{q}}^2 dM_{q\bar{q}}'^2 dM_{q\bar{q}}'^2}{\pi^3} \cdot \frac{dM^2}{\pi} \frac{d^4 \kappa_1}{i(2\pi)^4} \cdot \frac{G_A(M_{q\bar{q}}^2) d\Phi_2(P; k_q, k_{\bar{q}})}{M_{q\bar{q}}^2 - \mu_A^2} \\ \times \frac{d\Phi_1(P''; k_q'', k_{\bar{q}})}{M_{q\bar{q}}'^2 - (P_A + \kappa_1)^2 - i0} \cdot \frac{d\Phi_1(P'; k_q', k_{\bar{q}}) G_A(M_{q\bar{q}}'^2)}{M_{q\bar{q}}'^2 - \mu_A^2} S_I^{(q)} \frac{g^2 \hat{a}(\kappa_{1\perp}^2, \kappa_{2\perp}^2, M^2)}{M^2 - (P_B - \kappa_1^2)^2 - i0}. \quad (C.1)$$

The detailed presentation of the spectral integration technique and its application to the description of composite systems can be found in [48].  $G_A$  is the vertex function for the transition  $meson A \rightarrow q\bar{q}$ ;  $d\Phi_2$  and  $d\Phi_1$  are the phase spaces of the  $q\bar{q}$  intermediate states:

$$d\Phi_2(P; k_q, k_{\bar{q}}) = \frac{1}{2} \frac{d^3 k_q}{(2\pi)^3 2k_{q0}} \frac{d^3 k_{\bar{q}}}{(2\pi)^3 2k_{\bar{q}}} (2\pi)^4 \delta^4(P - k_q - k_{\bar{q}}), \\ d\Phi_1(P'; k_q', k_{\bar{q}}) = \frac{1}{2} \frac{d^3 k_q'}{(2\pi)^3 2k_{q0}'} \delta^4(P' - k_q' - k_{\bar{q}}). \quad (C.2)$$

Here  $P$  and  $P'$  stand for the total four-momenta of the intermediate states with invariant masses  $M_{q\bar{q}}$  and  $M_{q\bar{q}}'$ :  $P^2 = M_{q\bar{q}}^2$  and  $P'^2 = M_{q\bar{q}}'^2$ . To introduce the light–cone variables, the centre-of-mass system of the colliding particles  $A$  and  $B$  is the most suitable. Using the momentum notation  $p = (p_0, \vec{p}_\perp, p_z)$ , one has for  $P_A$  and  $P_B$ :

$$P_A = (p + \frac{\mu_A^2}{2p}, 0, p), \quad P_B = (p + \frac{\mu_B^2}{2p}, 0, -p). \quad (C.3)$$



The factor  $S_I^{(q)}$  is defined by the spin variables of quarks:

$$S_I^{(q)} = -\text{Sp} \left[ \Gamma_A (\hat{k}'_1 + m) \hat{n} (\hat{k}''_1 + m) \hat{n} (\hat{k}_1 + m) \Gamma_A (-\hat{k}_2 + m) \right], \quad (C.4)$$

where  $\Gamma_A$  is the spin-dependent factor for the vertex  $A \rightarrow q\bar{q}$ , for example,  $\Gamma_A = \gamma_5$  for meson, and  $\hat{n}$  quark–gluon vertex:

$$\hat{n} = \gamma_\alpha n_\alpha, \quad n = \frac{1}{2p}(1, 0, -1). \quad (C.5)$$

The gluon polarization  $n_\alpha$  which is parallel to  $P_B$  provides the main contribution into fermion loop related to meson A [49].

The phase space factors in terms of light–cone variables read:

$$\begin{aligned} d\Phi_2(P; k_q, k_{\bar{q}}) &= \frac{1}{(4\pi)^2} \frac{dx_q dx_{\bar{q}}}{x_q x_{\bar{q}}} \delta(1-x_q-x_{\bar{q}}) d^2 k_{q\perp} d^2 k_{\bar{q}\perp} \delta(\vec{k}_{q\perp} + \vec{k}_{\bar{q}\perp}) \delta \left( M_{q\bar{q}}^2 - \frac{m_{q\perp}^2}{x_q} - \frac{m_{\bar{q}\perp}^2}{x_{\bar{q}}} \right), \\ d\Phi_1(P'; k'_q, k_{\bar{q}}) &= \pi \frac{dx'_q}{x'_q} \delta(1-x'_q-x_{\bar{q}}) d^2 k'_{q\perp} \delta(\vec{k}'_{q\perp} + \vec{k}_{\bar{q}\perp} - \vec{q}_\perp) \delta \left( M_{q\bar{q}}'^2 + \vec{q}_\perp^2 - \frac{m_{q\perp}'^2}{x'_q} - \frac{m_{\bar{q}\perp}^2}{x_{\bar{q}}} \right), \\ d\Phi_1(P''; k''_q, k_{\bar{q}}) &= \pi \frac{dx''_q}{x''_q} \delta(1-x''_q-x_{\bar{q}}) d^2 k''_{q\perp} \delta(\vec{k}''_{q\perp} + \vec{k}_{\bar{q}\perp} - \vec{\kappa}_{1\perp}) \delta \left( M_{q\bar{q}}''^2 + \vec{\kappa}_{1\perp}^2 - \frac{m_{q\perp}''^2}{x''_q} - \frac{m_{\bar{q}\perp}^2}{x_{\bar{q}}} \right). \end{aligned} \quad (C.6)$$

Here  $x_q = k_{qz}/p$  and  $m_{q\perp}^2 = m^2 + k_{q\perp}^2$ . An important point is that  $\kappa_z/p$  is small at large  $p$ : it follows from the constraint  $M^2 \ll s$  for three-reggeon diagrams. The integration over  $M_{q\bar{q}}^2$ ,  $M_{q\bar{q}}'^2$ ,  $M_{q\bar{q}}''^2$  and the substitution  $(M^2 - (P_N - \kappa_1)^2 - i0)^{-1} \rightarrow i\pi \delta(M^2 - (P_B - \kappa_1)^2)$  (see (C.7)) give:

$$\begin{aligned} A^{(P)}(s, q_\perp^2) &= \frac{1}{4\pi} \int_0^1 \frac{dx}{x(1-x)^3} \int \frac{d^2 k_\perp}{(2\pi)^2} \cdot \frac{G_A(M_{q\bar{q}}^2)}{M_{q\bar{q}}^2 - \mu_A^2} \frac{G_A(M_{q\bar{q}}'^2)}{M_{q\bar{q}}'^2 - \mu_A^2} \\ &\times \int \frac{d\kappa_{10} d\kappa_{1z} d^2 \kappa_{1\perp}}{(2\pi)^4} S_I^{(q)} \frac{g^2 \hat{a}_{\text{PGG}}(\kappa_{1\perp}^2, \kappa_{2\perp}^2, -2p(\kappa_{10} + \kappa_{1z}))}{M_{q\bar{q}}''^2 - 2p(\kappa_{10} - \kappa_{1z}) - i0}, \end{aligned} \quad (C.7)$$

where  $x_{\bar{q}} \equiv x$ ,  $\vec{k}_{\bar{q}\perp} \equiv k_\perp$  and

$$M_{q\bar{q}}^2 = \frac{m^2 + k_\perp^2}{x(1-x)}, \quad M_{q\bar{q}}'^2 = \frac{m^2 + (\vec{k}_\perp - x\vec{q}_\perp)^2}{x(1-x)}, \quad M_{q\bar{q}}''^2 = \frac{m^2 + (\vec{k}_\perp - x\vec{\kappa}_{1\perp})^2}{x(1-x)}. \quad (C.8)$$

The integration over  $\kappa_- = \kappa_{10} - \kappa_{1z}$  is equivalent to the substitution  $(M_{q\bar{q}}''^2 - 2p\kappa_- - i0)^{-1} \rightarrow \frac{i\pi}{p} \delta(\kappa_-)$ , so we have

$$\begin{aligned} A^{(P)}(s, q_\perp^2) &= \frac{1}{4\pi} \int_0^1 \frac{dx}{x(1-x)^3} \int \frac{d^2 k_\perp}{(2\pi)^2} \cdot \frac{G_A(M_{q\bar{q}}^2)}{M_{q\bar{q}}^2 - \mu_A^2} \frac{G_A(M_{q\bar{q}}'^2)}{M_{q\bar{q}}'^2 - \mu_A^2} S_I^{q\bar{q}} \\ &\times \int \frac{d\kappa_+ d^2 \kappa_\perp}{(2\pi)^3} \cdot \frac{ig^2}{4p} \hat{a}_{\text{PGG}}(\kappa_{1\perp}^2, \kappa_{2\perp}^2, 2p\kappa_+). \end{aligned} \quad (C.9)$$

The factor  $G_A(M_{q\bar{q}}^2)/(M_{q\bar{q}}^2 - \mu_A^2)$  determines the wave function of meson  $A$ . The pion vertex  $G_\pi(M_{q\bar{q}}^2)$  has been found in [48] from the experimental data on pion form factor.

The factor  $S_I^q$  is given by (C.4). One can re-write it, using the equality  $\hat{n}\hat{n} = 0$ , as follows:

$$S_I^{(q)} = -2x_q \text{Sp} \left[ \Gamma_A(\hat{k}'_q + m) \hat{n}(\hat{k}_q + m) \Gamma_A(-\hat{k}_{\bar{q}} + m) \right], \quad (\text{C.10})$$

$\hat{n}$  being a spin-dependent quark–pomeron vertex.

**b. The pomeron interacting with antiquark.** When two reggeized gluons interact with antiquark, the spin-dependent part of the loop diagram reads:

$$\begin{aligned} S_I^{(\bar{q})} &= -\text{Sp} \left[ \Gamma_A(\hat{k}_q + m) \Gamma_A(-\hat{k}_{\bar{q}} + m) \hat{n}(-\hat{k}_{\bar{q}}'' + m) \hat{n}(-\hat{k}'_{\bar{q}} + m) \right] \\ &= -2x_{\bar{q}} \text{Sp} \left[ \Gamma_A(\hat{k}_q + m) \Gamma_A(-\hat{k}_{\bar{q}} + m) (-\hat{n})(-\hat{k}'_{\bar{q}} + m) \right]. \end{aligned} \quad (\text{C.11})$$

The antiquark–pomeron vertex is equal to  $-\hat{n}$ .

The momentum-dependent part of the loop diagram is determined by (C.9), with the re-definitions  $x \rightarrow (1-x)$  and  $\vec{k}_\perp \rightarrow -\vec{k}_\perp$ .

**c. The pomeron interacting with quark and antiquark, Fig. 12b.** The diagram of Fig. 12b written as a spectral integral over the  $q\bar{q}$  invariant mass reads:

$$\begin{aligned} A^{(P)}(s, q_\perp^2) &= \int_{4m^2}^\infty \frac{dM_{q\bar{q}}^2 dM_{q\bar{q}}''^2 dM_{q\bar{q}}'^2}{\pi^3} \cdot \frac{dM^2}{\pi} \frac{d^4\kappa_1}{i(2\pi)^4} \cdot \frac{G_A(M_{q\bar{q}}^2) d\Phi_2(P; k_q, k_{\bar{q}})}{M_{q\bar{q}}^2 - \mu_A^2} \\ &\times \frac{d\Phi_1(P''; k'_q, k_{\bar{q}})}{M_{q\bar{q}}''^2 - (P_A + \kappa_1)^2 - i0} \cdot \frac{d\Phi_1(P'; k'_q, k'_{\bar{q}}) G_A(M_{q\bar{q}}'^2)}{M_{q\bar{q}}'^2 - \mu_A^2} S_{II} \frac{g^2 \hat{a}(\kappa_{1\perp}^2, \kappa_{2\perp}^2, M^2)}{M^2 - (P_B - \kappa_1^2) - i0} \end{aligned} \quad (\text{C.12})$$

The factor  $S_{II}$  is defined by the quark spin variables:

$$S_{II}^{(q)} = -\text{Sp} \left[ \Gamma_A(\hat{k}'_1 + m) \hat{n}(\hat{k}_1 + m) \Gamma_A(-\hat{k}_2 + m) \hat{n}(-\hat{k}'_2 + m) \right]. \quad (\text{C.13})$$

The phase space factors in terms of the light–cone variables read:

$$\begin{aligned} d\Phi_2(P; k_q, k_{\bar{q}}) &= \frac{1}{(4\pi)^2} \frac{dx_q dx_{\bar{q}}}{x_q x_{\bar{q}}} \delta(1-x_q-x_{\bar{q}}) d^2k_{q\perp} d^2k_{\bar{q}\perp} \delta(\vec{k}_{q\perp} + \vec{k}_{\bar{q}\perp}) \delta \left( M_{q\bar{q}}^2 - \frac{m_{q\perp}^2}{x_q} - \frac{m_{\bar{q}\perp}^2}{x_{\bar{q}}} \right), \\ d\Phi_1(P'; k'_q, k'_{\bar{q}}) &= \pi \frac{dx'_{\bar{q}}}{x'_{\bar{q}}} \delta(1-x'_q-x'_{\bar{q}}) d^2k'_{q\perp} \delta(\vec{k}'_{q\perp} + \vec{k}'_{\bar{q}\perp} - \vec{q}_\perp) \delta \left( M_{q\bar{q}}'^2 + \vec{q}_\perp^2 - \frac{m_{q\perp}'^2}{x'_q} - \frac{m_{\bar{q}\perp}'^2}{x'_{\bar{q}}} \right), \\ d\Phi_1(P''; k'_q, k_{\bar{q}}) &= \pi \frac{dx'_q}{x'_q} \delta(1-x'_q-x_{\bar{q}}) d^2k'_{q\perp} \delta(\vec{k}'_{q\perp} + \vec{k}_{\bar{q}\perp} - \vec{\kappa}_{1\perp}) \delta \left( M_{q\bar{q}}''^2 + \vec{\kappa}_{1\perp}^2 - \frac{m_{q\perp}'^2}{x'_q} - \frac{m_{\bar{q}\perp}^2}{x_{\bar{q}}} \right). \end{aligned} \quad (\text{C.14})$$

Integrating over  $M_{q\bar{q}}^2$ ,  $M_{q\bar{q}}'^2$ ,  $M_{q\bar{q}}''^2$  and  $M^2$ , one gets:

$$A^{(P)}(s, q_\perp^2) = \frac{1}{4\pi} \int_0^1 \frac{dx}{x^2(1-x)^2} \int \frac{d^2k_\perp}{(2\pi)^2} \cdot \frac{G_A(M_{q\bar{q}}^2)}{M_{q\bar{q}}^2 - \mu_A^2} \frac{G_A(M_{q\bar{q}}'^2)}{M_{q\bar{q}}'^2 - \mu_A^2}$$

$$\times \int \frac{d\kappa_{10} d\kappa_{1z} d^2\kappa_{\perp}}{(2\pi)^4} S_{II} \frac{(-g^2) \hat{a}_{\mathbf{PGG}}(\kappa_{1\perp}^2, \kappa_{2\perp}^2, -2p(\kappa_{10} + \kappa_{1z}))}{M_{q\bar{q}}'^2 - 2p(\kappa_{10} - \kappa_{1z}) - i0}. \quad (C.15)$$

The invariant masses squared in the intermediate states are:

$$M_{q\bar{q}}^2 = \frac{m^2 + k_{\perp}^2}{x(1-x)}, \quad M_{q\bar{q}}'^2 = \frac{m^2 + (\vec{k}_{\perp} - x\vec{q}_{\perp})^2}{x(1-x)}, \quad M_{q\bar{q}}''^2 = \frac{m^2 + (\vec{k}_{\perp} - x\vec{\kappa}_{1\perp} - (1-x)\vec{\kappa}_{2\perp})^2}{x(1-x)}. \quad (C.16)$$

The integration over  $\kappa_{-} = \kappa_{10} - \kappa_{1z}$  is equivalent to the substitution  $(M_{q\bar{q}}''^2 - 2p\kappa_{-} - i0)^{-1} \rightarrow \frac{i\pi}{p} \delta(\kappa_{-})$ , so we have

$$\begin{aligned} A^{(P)}(s, q_{\perp}^2) &= -\frac{1}{4\pi} \int_0^1 \frac{dx}{x(1-x)^3} \int \frac{d^2k_{\perp}}{(2\pi)^2} \cdot \frac{G_A(M_{q\bar{q}}^2)}{M_{q\bar{q}}^2 - \mu_A^2} \frac{G_A(M_{q\bar{q}}'^2)}{M_{q\bar{q}}'^2 - \mu_A^2} \\ &\times \int \frac{d\kappa_{+} d^2\kappa_{\perp}}{(2\pi)^3} \cdot S_{II} \frac{ig^2}{4p} \hat{a}_{\mathbf{PGG}}(\kappa_{1\perp}^2, \kappa_{2\perp}^2, 2p\kappa_{+}). \end{aligned} \quad (C.17)$$

Here, in line with (C.10), the sign of  $\kappa_{+}$  is changed:  $\kappa_{+} = -\kappa_{10} - \kappa_{1z}$ .

## References

- [1] V.N. Gribov, Sov. Phys. JETP **14**, 478 (1961);  
G.F. Chew and S.C. Frautschi, Phys. Rev. Lett. **7**, 394 (1961)
- [2] A.B. Kaidalov and K.A. TerMartirosyan, Sov. J. Nucl. Phys. **39**, 979 (1984)
- [3] A. Donnachie and P.V. Landshoff, Nucl. Phys. B**231**, 189 (1984)
- [4] G.A. Schuler and T. Sjostrand, Phys. Rev. D**49**, 2257 (1994)
- [5] P.V. Landshoff, "Soft hadron reactions", in *QCD: 20 Years Later*, eds. P.M. Zerwas and H.A. Kastrup, (World Scientific, Singapore, 1993)
- [6] J. Gayler, in *Proceedings of the 28th International Conference on High Energy Physics*, edited by Z. Ajduk and A.K. Wroblewski, World Scientific, Singapore, 1997, pp. 608-612.
- [7] A.J. Askew, J. Kwiecinski, A.D. Martin, and P.J. Sutton, Phys. Rev. D**47**, 3775 (1993);  
*ibid*, D**49**, 4402 (1994);  
A.D. Martin, W.J. Stirling, and R.G. Roberts, Phys. Rev. D**50**, 6734 (1994)
- [8] V.V. Anisovich, E.M. Levin and M.G. Ryskin, Sov. J. Nucl. Phys. **29**, 674 (1979)
- [9] V.V. Anisovich, L.G. Dakhno, Nucl. Phys. (Proc. Suppl.) **B25** 247 (1992)
- [10] L.G. Dakhno, "Perturbative QCD-pomeron and high-energy hadronic diffractive cross sections", in *HADRON-94, Proceedings of the Workshop on Soft Physics, Sept. 7-11, 1994*, Kiev, 1994, p. 181;  
V.V. Anisovich, L.G. Dakhno, and V.A. Nikonov, "QCD-motivated pomeron and high energy hadronic diffractive cross sections", hep-ph/9511211;  
L.G. Dakhno, "Perturbative QCD-pomeron and high-energy hadronic diffractive cross sections", in *Frontiers in Strong Interactions* Proceedings of VI Blois Workshop, ed. by P. Chiapetta, M. Hagenauer and J. Tran Thanh Van (Edition Frontière, Gif-sur-Yvette, 1995) p. 189;  
V.V. Anisovich, L.G. Dakhno, and V.A. Nikonov, Phys. of Atomic Nuclei **59**, 702 (1996);  
L.G. Dakhno, "Colour screening in diffractive processes", in *Recent Advances in Hadron Physics*, Proceedings of VII Blois Workshop, Seoul, Korea, 10-14 June, ed. by Kyungsik Kang, Sung Ku Kim, Choonkyu Kim, World Scientific, Singapore, 1998, pp. 73-76.
- [11] J.P. Burq et al., Nucl. Phys. B**217** 285 (1983);  
Sh. Shukla "High Energy Elastic and Diffractive Scattering", preprint FERMILAB-Conf-92/232, 1992
- [12] V.V. Anisovich, L.G. Dakhno, and V.A. Nikonov, Phys. Rev. D**44**, 1385 (1991)

- [13] G. Parisi and R. Petronzio, Phys. Lett. **B94**, 51 (1980)
- [14] M. Consoli, J.H. Field, Phys. Rev. D**49**, 1293 (1994)
- [15] G.S. Bali et al. Phys. Lett. **B309**, 378 (1993)
- [16] J. Sexton, A. Vaccarino, and D. Weingarten, Phys. Rev. Lett. **75**, 4563 (1997)
- [17] V.V. Anisovich, Yu.D. Prokoshkin, and A.V. Sarantsev, Phys. Lett. **B389**, 388 (1996)
- [18] A.V. Anisovich, V.V. Anisovich, and A.V. Sarantsev, Phys. Lett. **B395**, 123 (1997)
- [19] V.V. Anisovich, S.M. Gerasyuta, A.V. Sarantsev, Int. Journal of Mod. Phys. **A6**, 625 (1991)
- [20] J.H. Field, Int. Journal of Mod. Phys. **A9**, 3283 (1994)
- [21] D.B. Leinweber et al. Phys. Rev. D**58**: 031501 (1998)
- [22] V.V. Anisovich, "Strong-interaction processes at high energies and quark-parton model", in *Proceedings of IX PNPI Winter School: Particles and Nuclei*, part 3, Leningrad, 1974, p. 106
- [23] V.V. Anisovich, "Constituent quarks and partons in soft processes", Section 6, in *Proceedings of XIV PNPI Winter School, Particles and Nuclei*, Leningrad, 1979, p. 4-81
- [24] V.V. Anisovich, M.N. Kobrinsky, J. Nyiri and Yu.M. Shabelski, in *Quark Model and High Energy Collisions* (World Scientific, Singapore, 1985)
- [25] P.V. Landshoff and O. Nachtmann, Z. Phys. **C35**, 405 (1987)
- [26] F.E. Low, Phys. Rev. D**12**, 163 (1975);  
S. Nussinov, Phys. Rev. Lett. **34**, 1286 (1975), Phys. Rev. D**14**, 246 (1976)
- [27] P. Jain, B. Pire, and J. Ralston, Physics Report **271**, 67 (1996)
- [28] J.F. Gunion and D.E. Soper, Phys. Rev. D**15**, 2617 (1977)
- [29] N.N. Nikolaev, B.Z. Kopeliovich, I.K. Potashnikova, Phys. Rev. D**39**, 769 (1989)
- [30] L.N. Lipatov, Sov. Phys. JETP **63**, 904 (1986)
- [31] J. Bartels et al. Phys. Lett. **B348**, 589 (1995)
- [32] A.H. Mueller and W.K. Tang, Phys. Lett. **B284**, 123 (1992)
- [33] E.A. Kuraev, L.N. Lipatov, and V.S. Fadin, Sov. Phys. JETP **44**, 443, (1976)
- [34] V.M. Braun and Ju.M. Shabelski, Int. J. Mod. Phys. A **3**, 2417 (1988)

- [35] Ya.Ya. Balitsky and L.N. Lipatov, Sov. J. Nucl. Phys. **28**, 882, (1978)
- [36] V.S. Fadin, M.I. Kotsky, and L.N. Lipatov, Phys. Lett. **B415** 97 (1997)
- [37] V.S. Fadin and L.N. Lipatov, in *PNPI Research Report*, Russian Academy of Science, PNPI, 1997, p. 160-165.
- [38] S.S. Gershtein and A.A. Logunov, Yad. Fiz. **39**, 514, (1984)
- [39] B. Margolis, P. Valin, M. Block, F. Halzen, and R.S. Fletcher, Phys. Rev. D**41** , 978 (1990);  
R.S. Fletcher, T.K. Gaisser, and F. Halzen, Phys. Lett. **B298**, 442 (1993)
- [40] J. Pumplin, Phys. Lett. **B276**, 517 (1992); **B289**, 449 (1992)
- [41] G. t'Hooft, Nucl. Phys. **B75**, 461 (1974);  
G. Veneziano, Nucl. Phys. **B117**, 519 (1976).
- [42] ZEUS Collaboration: M. Rocco, in *Proc. of 29th Rencontre de Moriond, March 1994* ed. J. Tran Thanh Van (Edition Frontière, Gif-sur-Ivette, 1995);  
H1-Collaboration: K. Mueller, in *Proc. of 29th Rencontre de Moriond, March 1994* ed. J. Tran Thanh Van (Edition Frontière, Gif-sur-Ivette, 1995)
- [43] A. Donnachie, P.V. Landshoff, Phys. Lett. **B437** 408 (1998)
- [44] V.V. Anisovich, L.G. Dakhno, and M.M. Giannini, Physics of Atomic Nuclei **57**, 1071 (1994); Phys. Rev. **C49**, 3275 (1994)
- [45] G.D. Alkhazov, V.V. Anisovich, and P.E. Volkovitsky, *Diffractional hadron-nucleus interaction at high energies*, Chapters III and VII (Nauka, Leningrad, 1991)
- [46] T.T. Chou and C.N. Yang, Phys. Lett. **B244**, 113 (1990)
- [47] J.H. Weis, Phys. Rev. D**6** , 2823 (1972);  
V.V. Anisovich, L.G. Dakhno, and P.E. Volkovitsky, JETP **63** , 1576 (1972)
- [48] V.V. Anisovich, D.I. Melikhov, and V.A. Nikonov, Phys. Rev. D**52**, 5295 (1995)
- [49] G.V. Frolov, V.N. Gribov, L.N. Lipatov, Sov. J. Nucl. Phys. **12**, 543 (1971)

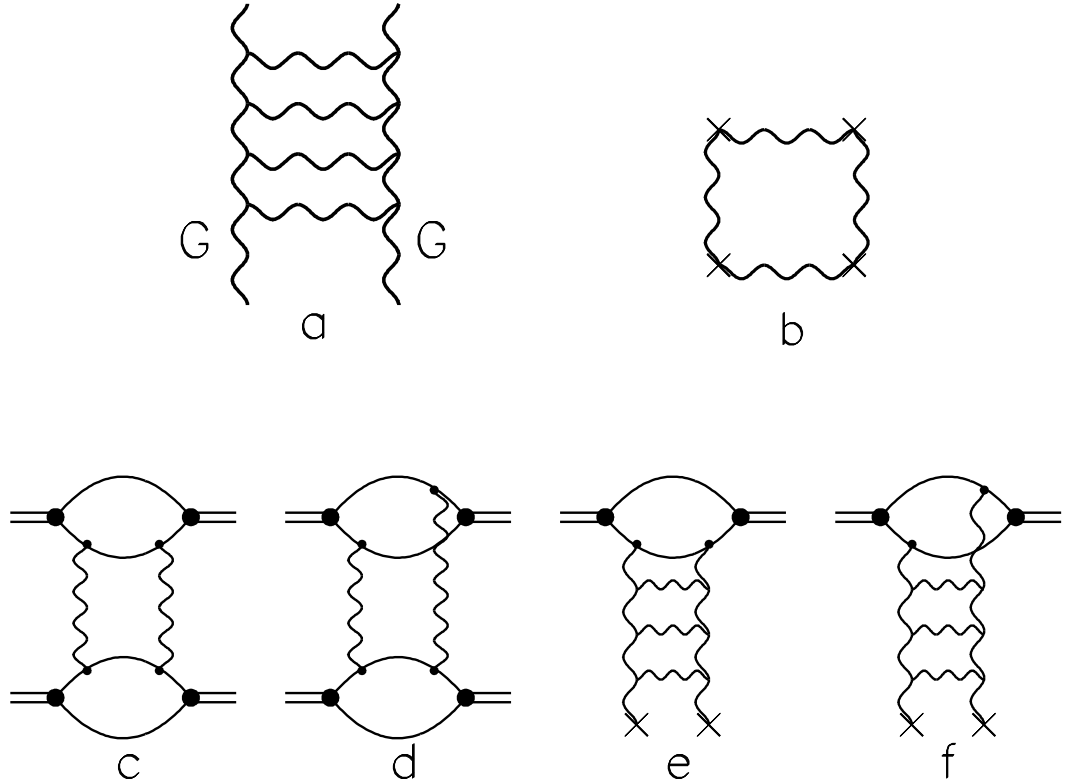


Figure 1: (a) Pomeron as gluon ladder; (b) gluon plaquet – a constructive element for the pomeron; (c)–(d) two-gluon exchange diagrams for meson–meson scattering: impulse approximation (c) and colour screening (d) diagrams; (e)–(f) pomeron–meson amplitude: impulse approximation (e) and colour screening (f) diagrams.

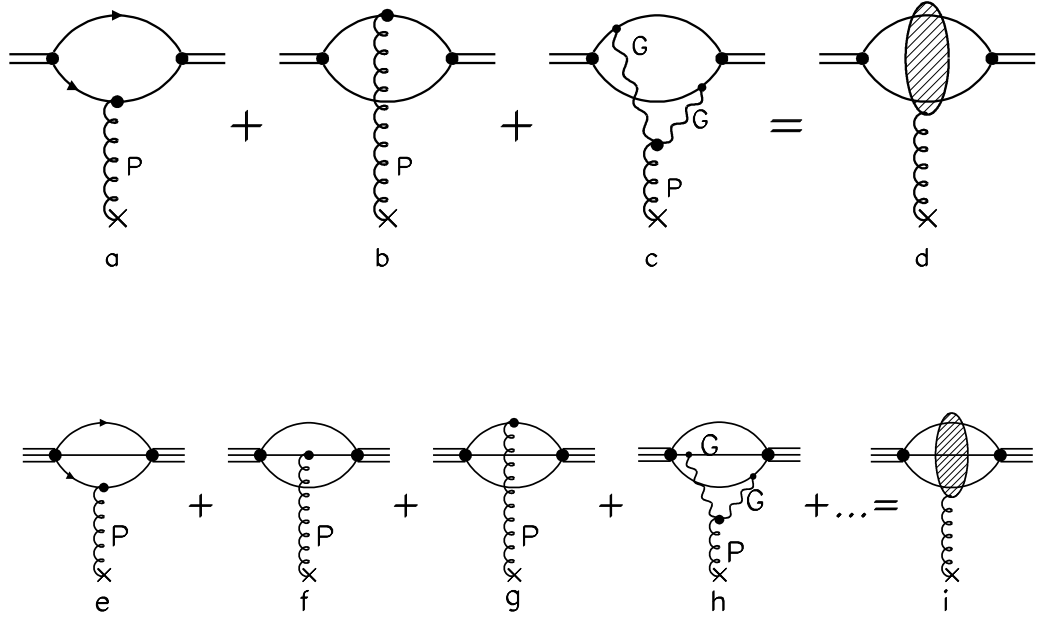


Figure 2: Diagrammatic representation of the pomeron–meson (a)–(d) and pomeron–proton (e)–(i) amplitudes, with  $\mathbf{P}$  being a pomeron and  $\mathbf{G}$  reggeized gluon. Three–reggeon diagrams  $\mathbf{P}\mathbf{G}\mathbf{G}$  provide the colour screening.

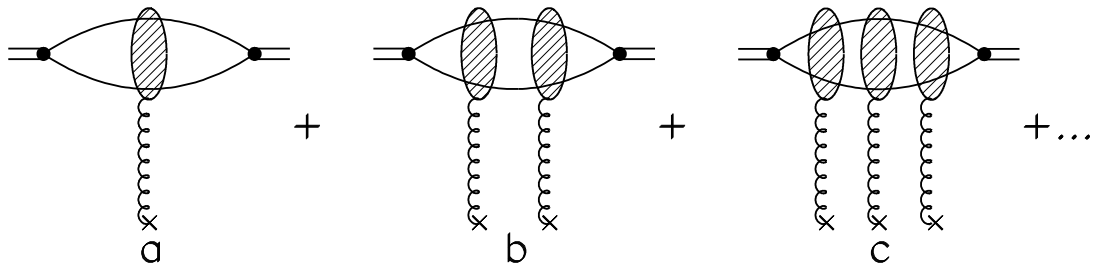


Figure 3: (a)–(c) Examples of multi-pomeron exchange diagrams, colour screening term included; the shaded block is that of Fig. 2d.



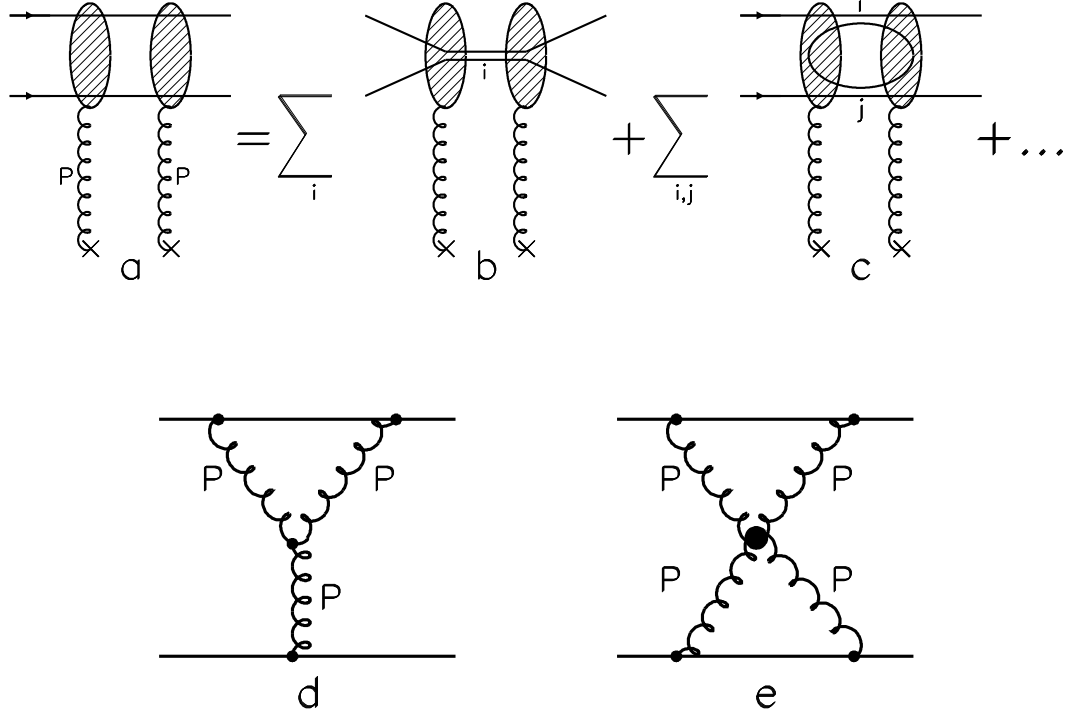


Figure 4: (a)–(c) Double rescattering diagrams: the intermediate  $q\bar{q}$  state is equivalent to the sum of all possible hadron states (b), (c), etc.; (d) the three-pomeron (**PPP**)  $t$ -channel exchange; (e) the four-pomeron exchange amplitude **PPPP**.

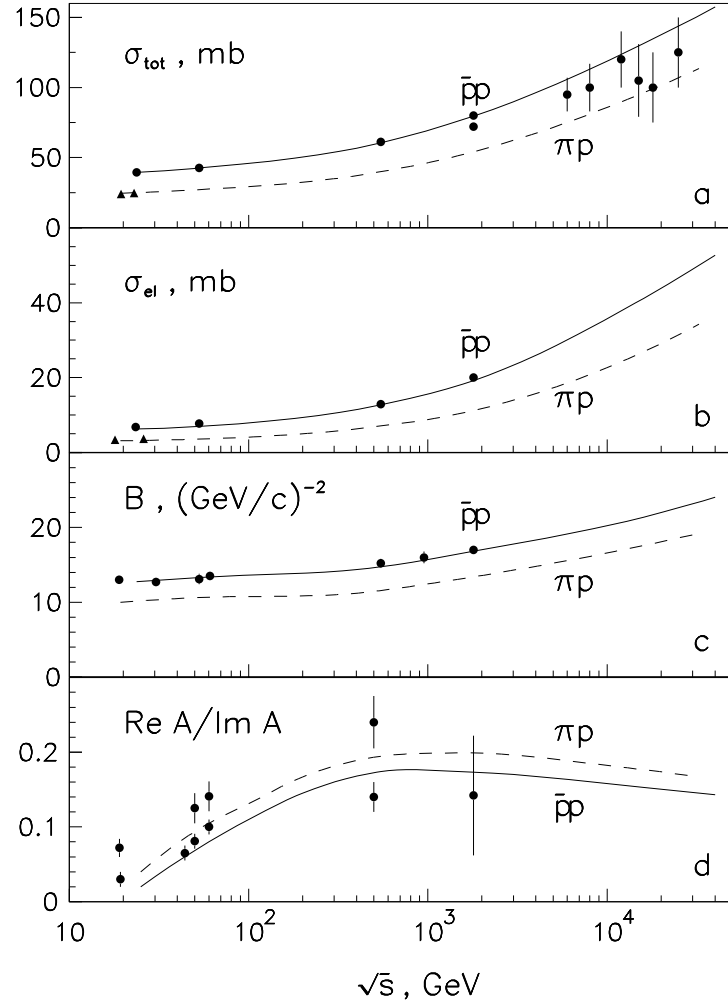


Figure 5: Description of experimental data in the energy range  $\sqrt{s} = 20 - 10^5$  GeV for (a) total and (b) elastic  $p\bar{p}(pp)$  and  $\pi p$  cross sections; (c) diffraction cone slope, and (d) the ratio real/imaginary parts of the amplitude.

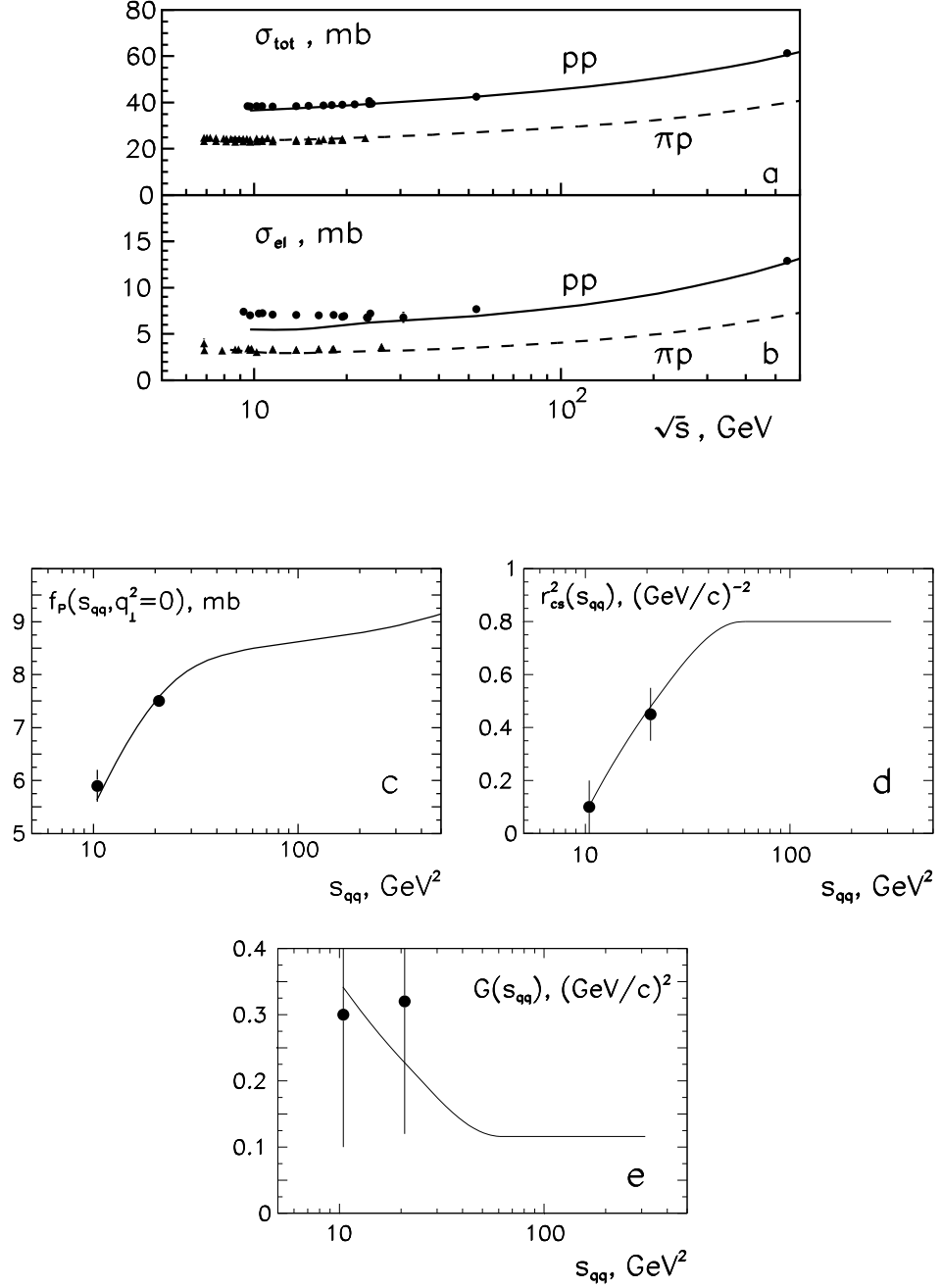


Figure 6: Description of experimental data in the energy range  $\sqrt{s} = 5 - 25$  GeV for (a) total and (b) elastic  $p\bar{p}(pp)$  and  $\pi p$  cross sections; (c)–(e) primary pomeron parameters as functions of the quark–quark energy squared,  $s_{qq}$ : (c) quark–pomeron coupling squared,  $f_P(s_{qq}, q_{\perp}^2 = 0)$ , (d) colour screening radius squared,  $r_{cs}^2$ , and (e) the pomeron slope  $G$ . The error bars show uncertainties of the parameter definition.

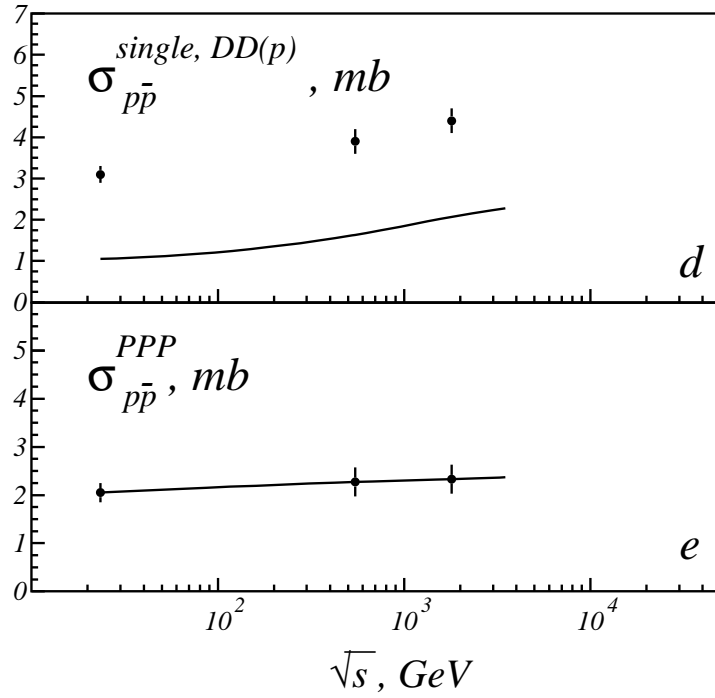
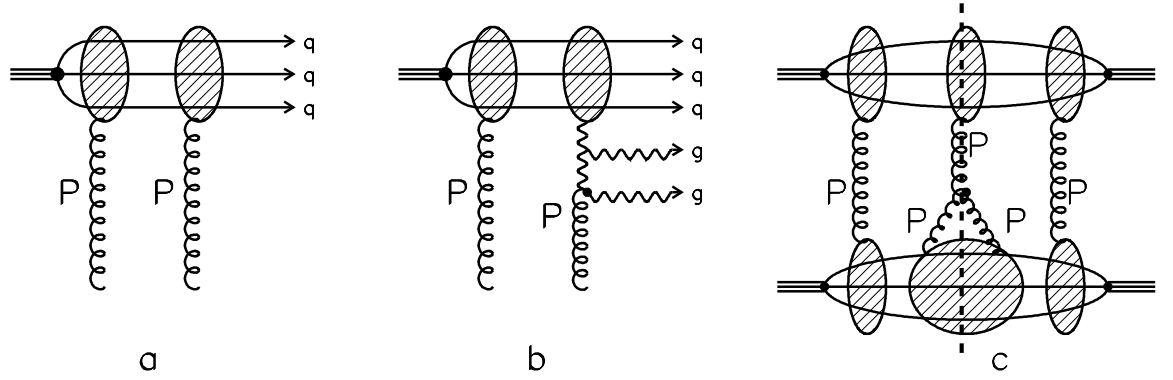


Figure 7: (a)-(b) Diagrams describing single diffraction dissociation: dissociation of a proton (a) and partly dissociating pomeron (b); (c) cutting of **PPP**-diagramm that gives the cross section with partly dissociating pomeron. (d) Experimental data for single diffractive dissociation of a proton, solid curve stands for the result of the calculation according to (20); (e) the estimated contribution for the dissociation of pomeron (three-pomeron diagram, Fig. 7a).

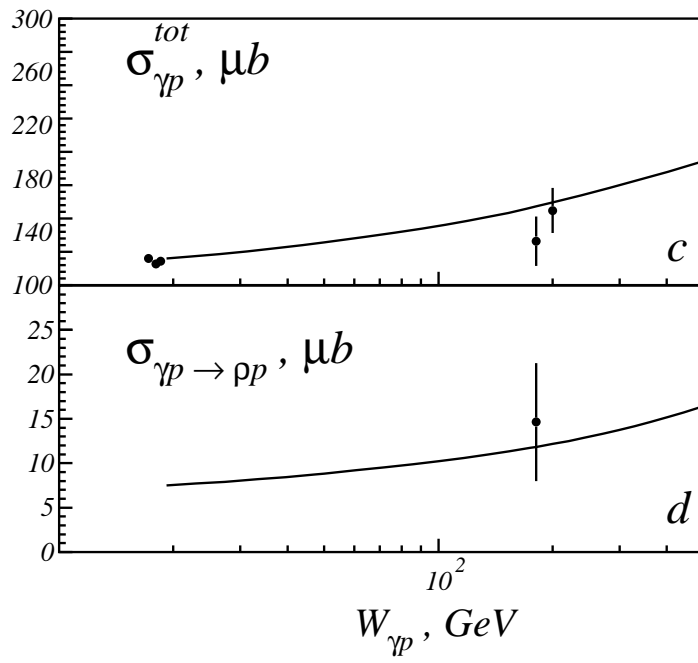
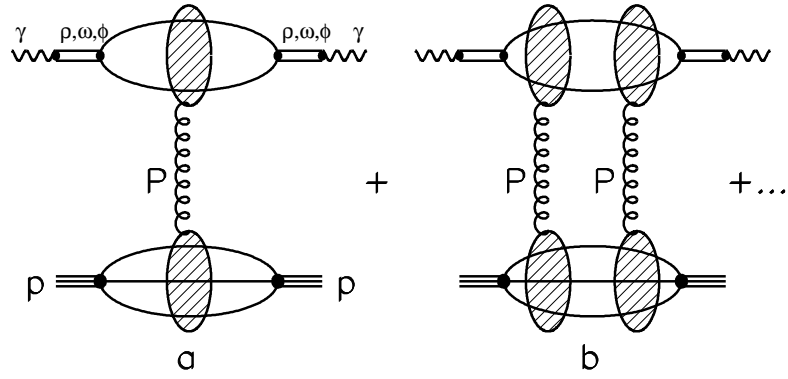


Figure 8: Photon-proton collisions: (a)–(b) diagrammatic representation of the  $\gamma p$  scattering amplitude; (c) description of the data on total cross section  $\gamma p$ , and (d) production of vector mesons  $\gamma p \rightarrow \rho p$ .

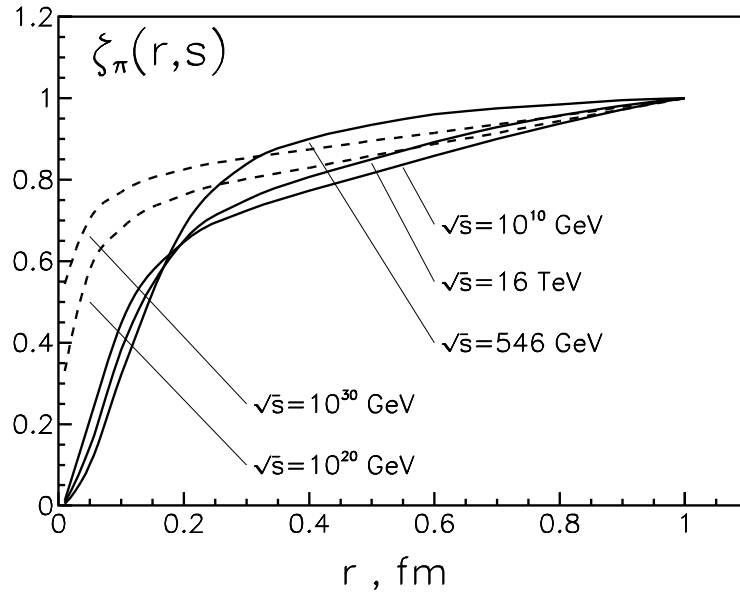


Figure 9: The pion profile function  $\zeta_\pi(r, s)$  depending on the interquark distance  $r = |\vec{r}_{1\perp} - \vec{r}_{2\perp}|$  at different energies  $\sqrt{s}$ .

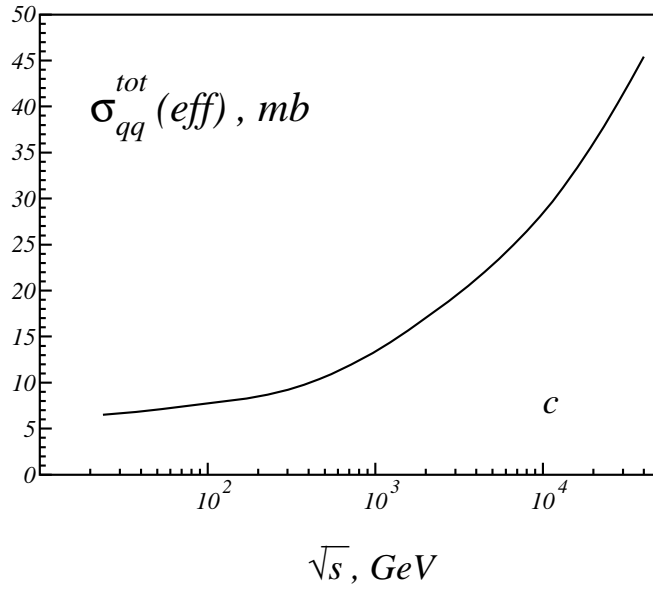
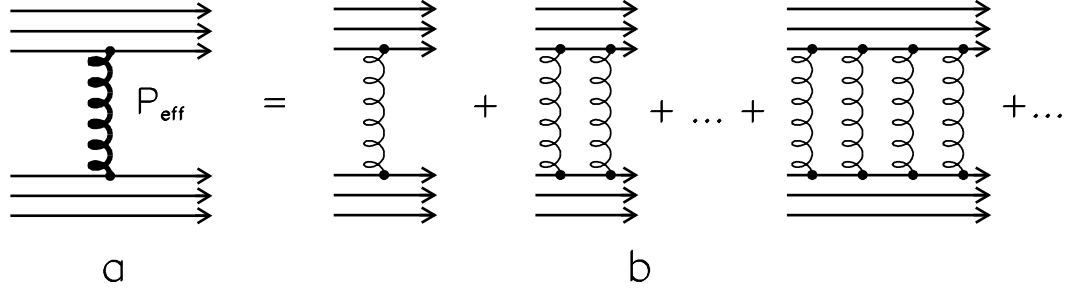


Figure 10: (a)–(b) Effective pomeron  $P_{eff}$  as a sum of the exchanges of primary pomerons and (c) the energy dependence of the quark–quark amplitude  $f_{qq}^{(P_{eff})} = \sigma_{qq}^{tot}(eff)$  due to the exchange of the effective pomeron.

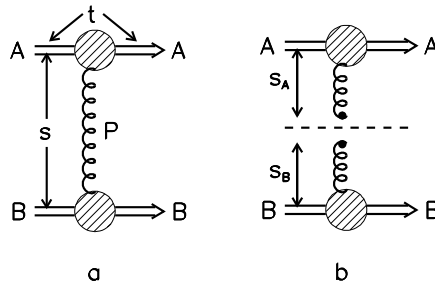


Figure 11: (a) Meson–meson scattering amplitude; (b) the pomeron cut enables to treat the pomeron–meson amplitudes separately.

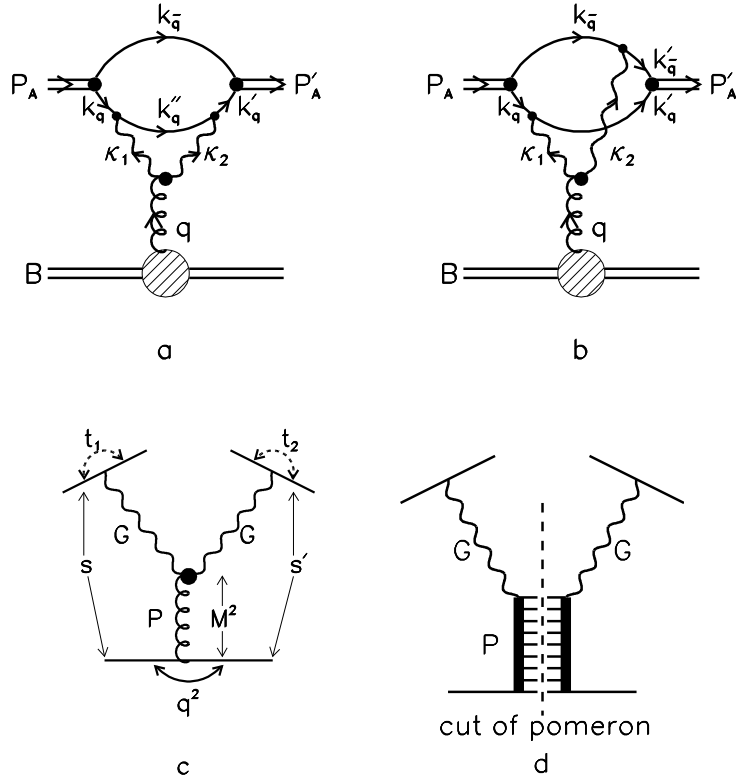


Figure 12: The **PGG** amplitude for coupling to (a) a single quark, (b) quark and anti-quark; (c) the used notations for the **PGG** diagram; (d) cutting along the pomeron line represents the discontinuity of the amplitude,  $disc_{M^2} A_{\mathbf{PGG}}$ .